Synthesis, Characterization, and Conformational Aspects of Chiral Cobalt(III) η^5-Indenyl and η^5-Cyclopentadienyl Phosphonate and Phosphinate Complexes

Zhongxin Zhou, Chet Jablonski,* and John Bridson[1]

Department of Chemistry, Memorial University of Newfoundland, St. John's, Newfoundland, Canada A1B 3X7

Received August 16, 1993®

Reactions of (η^5-Cp)Co(C_3F_7)(L)(I) (1: L = $P(OMe)_3$, PMe_3) and (η^5-indenyl)Co(R_f)(L)(I) (4: R_f = C_3F_7, C_6F_{13}; L = $P(OMe)_3$, PMe_3, $PPhMe_2$, PPh_2Me, $PPh(OMe)_2$) with $PR(OMe)_2$ (R = OMe, Ph) initially afford the corresponding labile ionic intermediates [(η^5-Cp)Co(C_3F_7)(L)($PR(OMe)_2$)]$^+$ (**2**) and [(η^5-indenyl)Co(R_f)(L)($PR(OMe)_2$)]$^+$ (**5**), respectively, which subsequently dealkylate with loss of MeI in benzene via Arbuzov rearrangement to give the phosphonate and phosphinate complexes (η^5-Cp)Co(C_3F_7)(L)(P(O)R(OMe)) (**3**) and (η^5-indenyl)Co(R_f)(L)(P(O)R(OMe)) (**6**) (R = OMe, Ph). In most cases intermediates **2** and **5** are directly observable by ^{1}H NMR in acetone-d_6. The solid-state structure of [(η^5-indenyl)Co(C_3F_7)($P(OMe)_3$)$_2$)]$^+SbF_6^-$ (**5a**α-**SbF$_6$**) was determined by X-ray diffraction. **5a**α-**SbF$_6$** crystallizes in the monoclinic system, space group $P2_1/c$ (No. 14), with a = 12.821(4) Å, b = 12.057(3) Å, c = 18.835(4) Å, β = 99.74(2)°, V = 2869(1) Å^3, Z = 4, and R = 0.055 (R_w = 0.039) for 1913 reflections with $I > 2.00\sigma(I)$. Crystal structures of several phosphonate and phosphinate derivatives establish characteristic conformational preferences in the solid state which are demonstrated by ^{1}H NOED data to persist in solution. Crystal data: **6b**α crystallizes in the monoclinic system, space group $P2_1/c$ (No. 14), with a = 8.235(2) Å, b = 16.983(3) Å, c = 15.795(2) Å, β = 101.88(1)°, V = 2161.6(7) Å^3, Z = 4, and R = 0.038 (R_w = 0.034) for 2455 reflections with $I > 3.00\sigma(I)$; **6b**β-1 crystallizes in the monoclinic system, space group $P2_1/c$ (No. 14), with a = 12.626(2) Å, b = 14.017(7) Å, c = 14.380(2) Å, β = 107.46(1)°, V = 2428(1) Å^3, Z = 4, and R = 0.051 (R_w = 0.040) for 2158 reflections with $I > 3.00\sigma(I)$; **6c**β-**2**·$CHCl_3$·2.85H_2O crystallizes in the monoclinic system, space group $C2/c$ (No. 15), with a = 21.794(8) Å, b = 15.214(2) Å, c = 21.115(3) Å, β = 92.33(2)°, V = 6995(3) Å^3, Z = 8, and R = 0.052 (R_w = 0.036) for 3961 reflections with $I > 2.00\sigma(I)$; **3b**β-1 crystallizes in the monoclinic system, space group $P2_1/c$ (No. 14), with a = 8.481(4) Å, b = 17.916(3) Å, c = 14.518(2) Å, β = 97.31(2)°, V = 2188(1) Å^3, Z = 4, and R = 0.036 (R_w = 0.033) for 2780 reflections with $I > 3.00\sigma(I)$. The dominant conformation places the highest *trans*-influence ligand, P(O)R(OMe), *anti* to the indenyl six-ring and staggers the substituents along the Co–P(O) bond with the phosphoryl P=O bond aligned *anti* to the indenyl or cyclopentadienyl plane. Empirical correlations between chromatographic relative R_f values, NMR parameters, and the relative configuration of the phosphinates, which provide a simple way to determine the stereochemistry of chiral cobaltiophosphinates, were established.

Introduction

Our previous studies[2-5] of Arbuzov-like dealkylations[6] using the Co–chiral aminophosphine substituted auxiliary CpCoX(PNH*)$^-$ (X = I, CF_3, C_3F_7; PNH* = *S*-(−)-Ph_2PNHC*H(Me)Ph) concluded that intramolecular P=O···H—N hydrogen bonding at the nascent phosphoryl oxygen site played an important role in Co*→P chiral induction by limiting conformational mobility. The stereochemistry of the major diastereomer was reliably predicted from the transition state which minimizes 1,3-diaxial interactions between the phosphonite substituent R and a pseudoaxial phenyl substituent of the aminophosphine, as shown in Scheme 1.

Attempts to assess the controlling effect of intramolecular hydrogen bonding in these reactions by studying analogs containing blocked, N-alkylated aminophosphine $Ph_2PN(R)C^*H(CH_3)Ph$ failed.[7] This paper examines Arbuzov dealkylations of $P(OMe)_3$ and the prochiral phosphonite $PPh(OMe)_2$ mediated by the isostructural Co–chiral auxiliaries [(η^5-Cp)Co(PMe_3)(C_3F_7)–]$^+$ and [(η^5-indenyl)Co(L)(R_f)–]$^+$ (L = PPh_nMe_{3-n} (n = 0–2), $PR(OMe)_2$ (R = Ph, OMe); R_f = C_3F_7, C_6F_{13}), which provide non-hydrogen-bonding templates for diastereoselective Arbuzov dealkylation. Solid-state and solution conformations are compared, and evidence for restricted rotation about the cobalt–indenyl and –P(O) bonds is presented.

Results and Discussion

Synthesis of Cobalt η^5-Cyclopentadienyl and η^5-Indenyl Phosphonate and Phosphinate Complexes.

* Abstract published in *Advance ACS Abstracts*, January 1, 1994.

(1) Crystallography Unit, Department of Chemistry, Memorial University.

(2) Brunner, H.; Jablonski, C. R.; Jones, P. G. *Organometallics* 1988, *7*, 1283–1292.

(3) Jablonski, C. R.; Burrow, T.; Jones, P. G. *J. Organomet. Chem.* 1989, *370*, 173–185.

(4) Jablonski, C. R.; Ma, H. Z.; Chen, Z.; Hynes, R. C.; Bridson, J. N.; Bubenik, M. P. *Organometallics* 1993, *12*, 917–926.

(5) Boone, B. J.; Jablonski, C. R.; Jones, P.; Newlands, M. J.; Yu, Y. *Organometallics* 1993, *12*, 3042–3050.

(6) Brill, T. B.; Landon, S. J. *Chem. Rev.* 1984, *84*, 577–585.

(7) Jablonski, C. R.; Ma, H. Z.; Hynes, R. C. *Organometallics* 1992, *11*, 2796–2802.

0276-7333/94/2313-0781$04.50/0 © 1994 American Chemical Society

Scheme 1

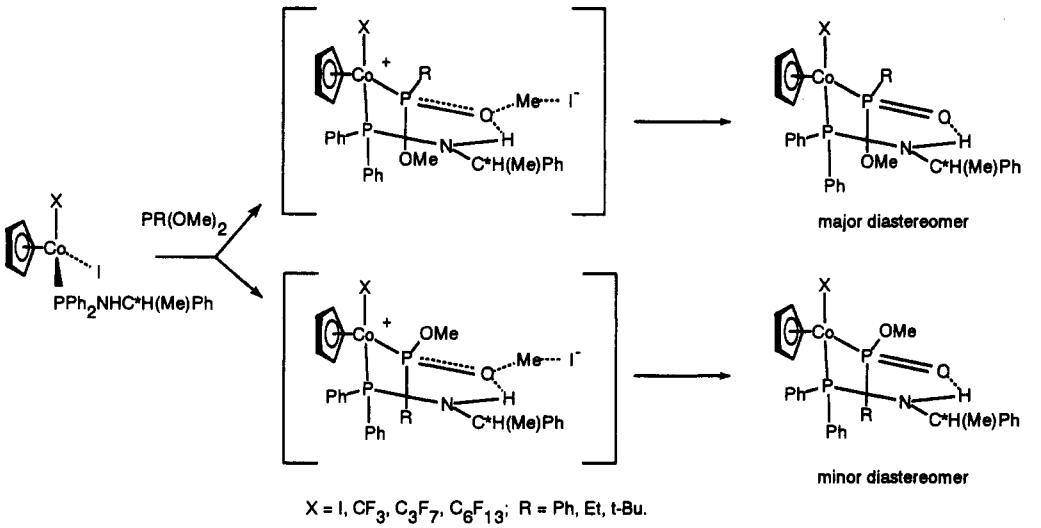

Scheme 2

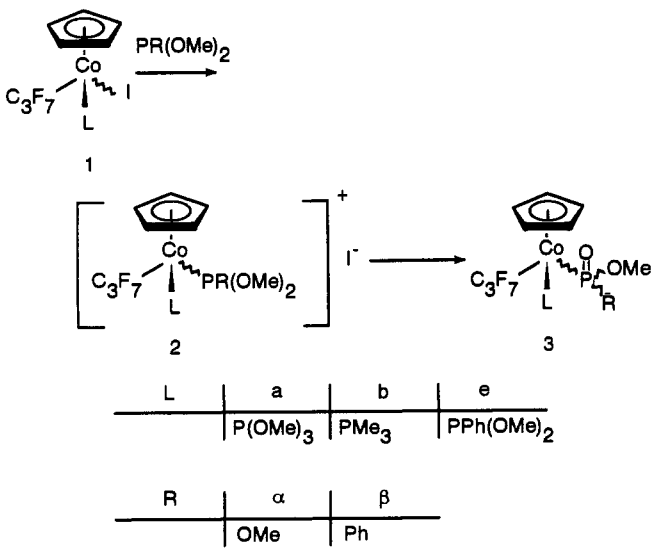

Phosphonate and P-chiral phosphinate targets were synthesized using the transition-metal Arbuzov reaction,[6] which involves sequential substitutions of the iodides 1 and 4 at cobalt and carbon (cf. Schemes 2 and 3). In our experience preferential substitution of labile CO in (η^5-Cp)Co(R_f(CO)(I) and (η^5-indenyl)Co(R_f)(CO)(I) by P-donor ligands[8-10] represents a more general synthetic route[2,11-14] to the required substrates 1 and 4 than oxidative addition of RI (R = I, R_f) to phosphine-substituted Co(I) complexes.[15] Treatment of 1 and 4 with $P(OMe)_3$ or $PPh(OMe)_2$ initially affords the corresponding labile ionic intermediates[6,16-21] [(η^5-Cp)Co(C_3F_7)(L)($PR(OMe)_2$)]$^+$ (2)

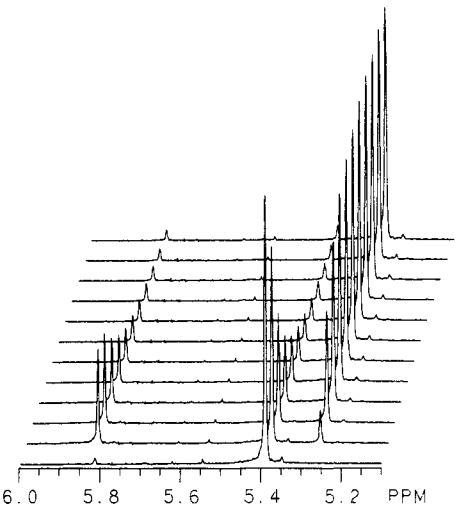

Figure 1. ^{1}H NMR spectra for the reaction between (η^5-Cp)Co(C_3F_7)($P(OMe)_3$)(I) (**1a**) and $P(OMe)_3$ in acetone-d_6 at 25 °C: $[\mathbf{1a}]_0 = 0.01568$ mol L^{-1}; $[P(OMe)_3]_0 = 0.1728$ mol L^{-1}; first spectrum recorded at $t = 550$ s; $\Delta = 1800$ s for remaining spectra.

and [(η^5-indenyl)Co(R_f)(L)($PR(OMe)_2$)]$^+$ (5), respectively, which rapidly dealkylate in nonpolar solvents to give good yields of the orange-yellow phosphonate and phosphinate complexes (η^5-Cp)Co(C_3F_7)(L)(P(O)(R)(OMe)) (3) and (η^5-indenyl)Co(R_f)(L)(P(O)(R)(OMe)) (6) (R = OMe, Ph), respectively (cf. Schemes 2 and 3). Physical and analytical data for the phosphonate and phosphinate complexes prepared are reported in Table 1.

Reactions of several η^5-Cp and η^5-indenyl complexes with $P(OMe)_3$ were followed by ^{1}H NMR at 25 °C in benzene-d_6 and in acetone-d_6. Only reactants (1 or 4) and products (3 or 6) were observable at 25 °C with benzene as solvent; however, a reaction intermediate was clearly detected by ^{1}H NMR for both series in acetone-d_6 at 25 °C (cf. Figures 1 and 2). For the reaction of **1a** with

(8) Brunner, H.; Riepl, G.; Benn, R.; Rufinska, A. *J. Organomet. Chem.* **1983**, *253*, 93–115.
(9) Brunner, H.; Rambold, W. *J. Organomet. Chem.* **1974**, *64*, 373–383.
(10) Brunner, H.; Doppelberger, J.; Dreischl, P.; Moellenberg, T. *J. Organomet. Chem.* **1977**, *139*, 223–233.
(11) Jablonski, C.; Zhou, Z.; Bridson, J. N. *J. Organomet. Chem.* **1992**, *429*, 379–389.
(12) Jablonski, C. R.; Zhou, Z. *Can. J. Chem.* **1992**, *70*, 2544–2551.
(13) Zhou, Z.; Jablonski, C. R.; Bridson, J. N. *J. Organomet. Chem.* **1993**, *461*, 215–227.
(14) Zhou, Z.; Jablonski, C. R.; Bridson, J. N. *Organometallics* **1993**, *12*, 3677–3687.
(15) King, R. B. *Inorg. Chem.* **1965**, *1*, 82–87.
(16) Haines, R. J.; DuPreez, A. L.; Marais, L. L. *J. Organomet. Chem.* **1971**, *28*, 405–413.
(17) Klăui, W.; Buchholz, E. *Inorg. Chem.* **1988**, *27*, 3500–3506.
(18) Neukomm, H.; Werner, H. *J. Organomet. Chem.* **1976**, *108*, C26–C28.
(19) Nakazawa, H.; Kadoi, Y.; Mizuta, T.; Miyoshi, K.; Yoneda, H. *J. Organomet. Chem.* **1989**, *366*, 333–342.
(20) Nakazawa, H.; Kadoi, Y.; Miyoshi, K. *Organometallics* **1989**, *8*, 2851–2856.
(21) Sullivan, R. J.; Bao, Q. B.; Landon, S. J.; Rheingold, A. L.; Brill, T. B. *Inorg. Chim. Acta* **1986**, *111*, 19–24.

Scheme 3

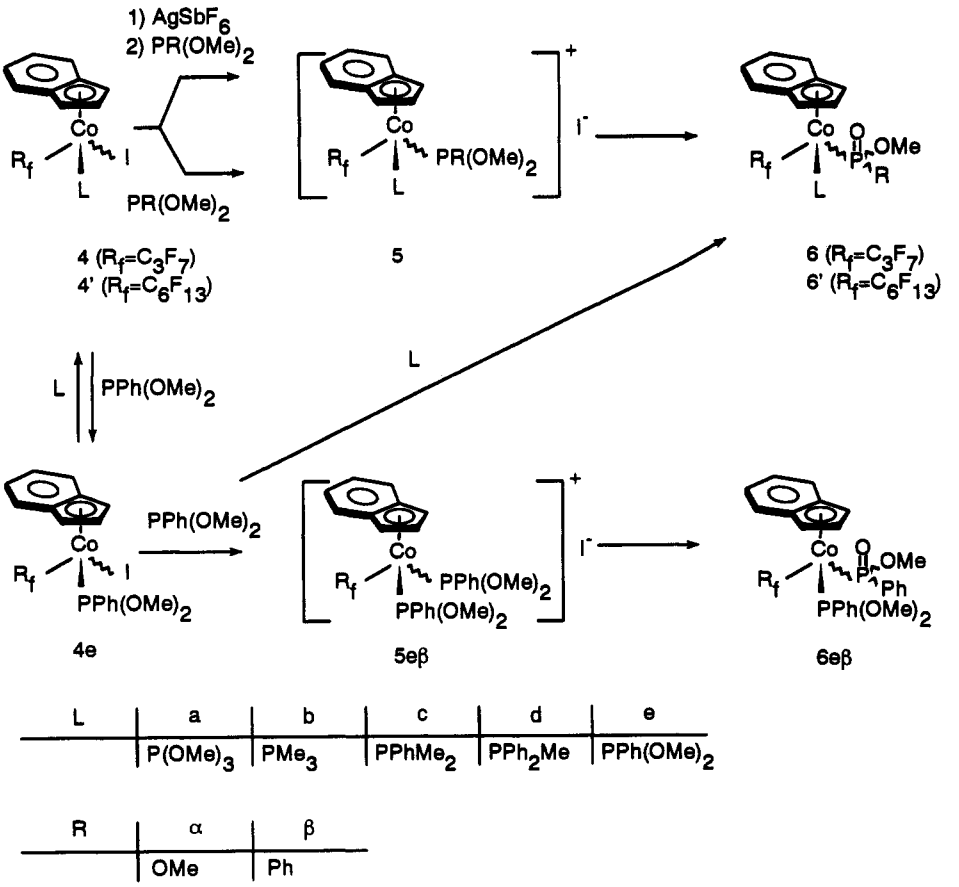

Table 1. Physical Properties of Cobalt(III) η^5-Cyclopentadienyl and η^5-Indenyl Complexes

compd	formula	appearance	mp[a] (°C)	anal. calcd (found) C, H (%)
1b	$(C_5H_5)Co(C_3F_7)(I)(PMe_3)$	dark blue powder	197–199	26.64 (26.74), 2.84 (2.74)
1b′	$[(C_5H_5)Co(C_3F_7)(PMe_3)_2]^+I^-$	orange plate	195–197	29.39 (28.93), 4.05 (3.95)
3aα	$(C_5H_5)Co(C_3F_6)(P(OMe)_3)(P(O)(OMe)_2)$	orange microcryst	102–104	29.68 (30.06), 3.83 (3.69)
3bα	$(C_5H_5)Co(C_3F_7)(PMe_3)(P(O)(OMe)_2)$	yellow microcryst	136–138	32.65 (32.49), 4.22 (4.45)
5aα-SbF_6	$[(C_9H_7)Co(C_3F_7)(P(OMe)_3)_2]^+SbF_6^-$	orange rect plate	176–177	26.14 (26.17), 3.05 (3.00)
6aα	$(C_9H_7)Co(C_3F_7)(P(OMe)_3)(P(O)(OMe)_2)$	red powder	87–88	35.44 (35.51), 3.85 (3.96)
6′aα	$(C_9H_7)Co(C_6F_{13})(P(OMe)_3)(P(O)(OMe)_2)$	red powder	48–50	33.08 (33.03), 3.05 (2.82)
6bα	$(C_9H_7)Co(C_3F_7)(PMe_3)(P(O)(OMe)_2)$	deep red prism	151–153	38.66 (38.67), 4.20 (4.35)
6cα	$(C_9H_7)Co(C_3F_7)(PPhMe_2)P(O)(OMe)_2)$	red powder	134–135	44.66 (44.63), 4.10 (4.14)
3bβ-1	$(C_5H_5)Co(C_3F_7)(PMe_3)(P(O)Ph(OMe))$	orange prism	185–187	41.24 (41.35), 4.23 (4.16)
3bβ-2	$(C_5H_5)Co(C_3F_7)(PMe_3)(P(O)Ph(OMe))$	orange microcryst	143–144	41.24 (40.95), 4.23 (4.21)
6bβ-1	$(C_9H_7)Co(C_3F_7)(PMe_3)(P(O)Ph(OMe))$	orange plate	160–161	46.01 (45.67), 4.21 (4.25)
6bβ-2	$(C_9H_7)Co(C_3F_7)(PMe_3)(P(O)Ph(OMe))$	red microcryst	101–104	46.01 (45.74), 4.21 (4.13)
6cβ-1	$(C_9H_7)Co(C_3F_7)(PPhMe_2)(P(O)Ph(OMe))$	red powder	145–146	50.96 (51.14), 4.12 (4.23)
6cβ-2	$(C_9H_7)Co(C_3F_7)(PPhMe_2)(P(O)Ph(OMe))$	red prism	98–101	
6dβ-1	$(C_9H_7)Co(C_3F_7)(PPh_2Me)(P(O)Ph(OMe))$	red powder	150–151	55.03 (54.88), 4.04 (4.15)
6dβ-2	$(C_9H_7)Co(C_3F_7)(PPh_2Me)(P(O)Ph(OMe))$	red powder		
6eβ-1	$(C_9H_7)Co(C_3F_7)(PPh(OMe)_2)(P(O)Ph(OMe))$	red powder	78–81	48.52 (48.45), 3.92 (3.92)
6eβ-2	$(C_9H_7)Co(C_3F_7)(PPh(OMe)_2)(P(O)Ph(OMe))$	red powder	90–93	48.52 (48.04), 3.92 (3.72)

[a] Sealed (N_2) capillary.

$P(OMe)_3$ the reactant (δ 5.40 ppm) diminishes, the intermediate **2a** (δ 5.81 ppm) builds and then decays, and the phosphonate product **3aα** increases (δ 5.27 ppm). Similarly, **4a** (H_1, δ 5.52; H_3, δ 6.27 ppm) is rapidly consumed on treatment with $P(OMe)_3$ to form the unstable intermediate **5aα** (H_3, H_1, δ 6.43; H_2, δ 5.95 ppm), which subsequently collapses to form the phosphonate **6aα** (H_2, δ 5.85; H_1, δ 5.40 ppm).

Reactions of **1** and **4** with prochiral $PPh(OMe)_2$ were more complicated, since diastereomers are possible. For **1b**, **4b**, and **4c** (cf. Schemes 2 and 3) the cationic intermediates $[(\eta^5\text{-Cp})Co(C_3F_7)(PMe_3)(PPh(OMe)_2)]^+$ (**2bβ**) and $[(\eta^5\text{-indenyl})Co(C_3F_7)(L)(PPh(OMe)_2)]^+$ (L = PMe_3 (**5bβ**), $PPhMe_2$ (**5cβ**)) were directly observed by ^1H NMR as a pair of diastereotopic O*Me* doublets at ca. 4.0–4.2 ppm with $^3J_{PH} \approx 10$ Hz in acetone-d_6 at 25 °C. Displaced I^- in the ion pair subsequently attacks at carbon in coordinated $PPh(OMe)_2$ to afford the two red-orange diastereomeric phosphinate complexes $(\eta^5\text{-Cp})Co(C_3F_7)(PMe_3)(P(O)Ph(OMe))$ (**3bβ-1,2**)[22] and $(\eta^5\text{-indenyl})Co(C_3F_7)(L)(P(O)Ph(OMe))$ (**6bβ-1,2** and **6cβ-1,2**), respectively.

The spectroscopic characterizations of the cationic intermediate phosphite and phosphonate species were confirmed by isolation and X-ray crystallographic study

(22) The designations -1 and -2 refer to diastereomers in order of decreasing chromatographic R_f values.

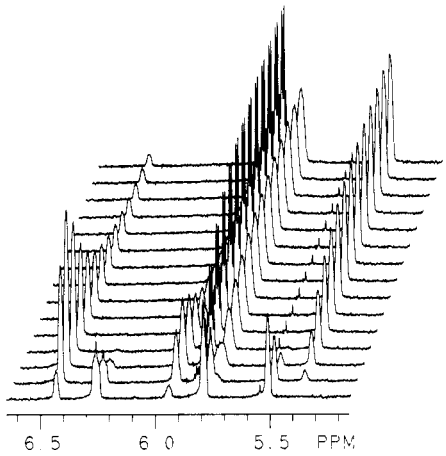

Figure 2. ^{1}H NMR spectra for the reaction between (η^5-indenyl)Co(C_3F_7)(P(OMe)$_3$)(I) (**4a**) and P(OMe)$_3$ in acetone-d_6 at 25 °C: [**4a**]$_0$ = 0.01566 mol L^{-1}, [P(OMe)$_3$]$_0$ = 0.1733 mol L^{-1}; first spectrum recorded at t = 425 s; Δt = 600 s for remaining spectra.

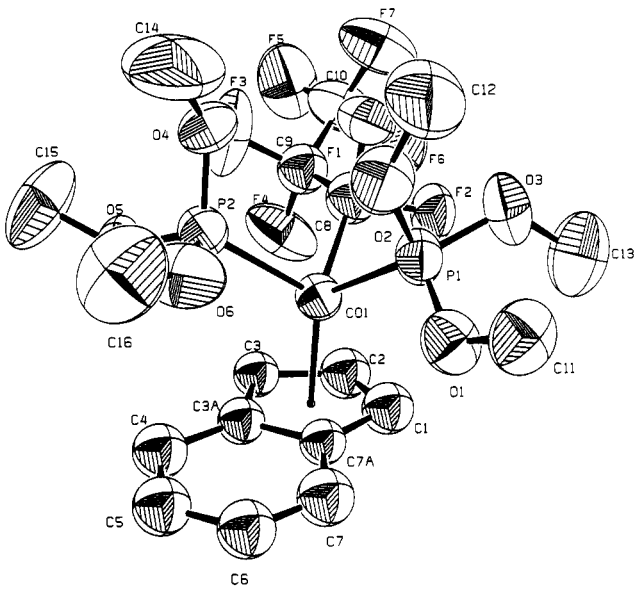

Figure 3. ORTEP representation of [(η^5-indenyl)Co(C_3F_7)(P(OMe)$_3$)$_2$]$^+$SbF$_6^-$ (**5a**α-SbF$_6$) (SbF$_6^-$ omitted for clarity).

of **5a**α-SbF$_6$ prepared by an independent route. Abstraction of iodide from **4a** with AgSbF$_6$ in acetone followed by reaction with 1 equiv of P(OMe)$_3$ gave a 95% yield of orange, crystalline [(η^5-indenyl)Co(C_3F_7)(P(OMe)$_3$)$_2$]$^+$SbF$_6^-$ (**5a**α-SbF$_6$). Treatment of **5a**α-SbF$_6$ with an acetone solution of LiI afforded phosphonate product **6a**α identical with that obtained by direct reaction of **4a** with P(OMe)$_3$ (cf. Scheme 3). The solid-state structure of **5a**α-SbF$_6$ (cf. Figure 3) consists of an unexceptional η^5-indenyl piano stool with approximate octahedral coordination geometry about cobalt. Interligand bond angles P(1)–Co(1)–P(2), P(1)–Co(1)–C(8), and P(2)–Co(1)–C(8) are all close to 90°. Atomic coordinates and selected bond lengths and angles are given in Tables 2 and 7.

Minor amounts of mixed, diastereomeric phosphonite/phosphinate species (η^5-Cp)Co(C_3F_7)(PPh(OMe)$_2$)(P(O)Ph(OMe)) (**3e**β-**1,2**) and (η^5-indenyl)Co(C_3F_7)(PPh(OMe)$_2$)(P(O)Ph(OMe)) (**6e**β-**1,2**), presumably the result of stepwise disubstitution of I$^-$ and L by PPh(OMe)$_2$ followed by Arbuzov dealkylation, were spectroscopically observed in the reaction of dimethyl phenylphosphonite with **1** and

Table 2. Atomic Coordinates for [(η^5-C_9H_7)Co(C_3F_7)(P(OMe)$_3$)$_2$]$^+$SbF$_6^-$ (5aα-SbF$_6$)

atom	x	y	z	B(eq) (Å^2)
Sb(1)	0.20043(8)	0.2001(1)	0.75701(6)	6.07(6)
Co(1)	0.7568(1)	0.2758(1)	0.53760(8)	4.08(9)
P(1)	0.8081(3)	0.1053(3)	0.5681(2)	5.1(2)
P(2)	0.6799(3)	0.2352(3)	0.4280(2)	5.3(2)
F(1)	0.5846(5)	0.1485(6)	0.5674(4)	5.9(4)
F(2)	0.6585(5)	0.2525(6)	0.6574(3)	5.9(4)
F(3)	0.4834(7)	0.3194(8)	0.5008(4)	9.4(5)
F(4)	0.5644(6)	0.4373(6)	0.5781(5)	8.4(5)
F(5)	0.3652(7)	0.3763(9)	0.5924(5)	10.3(7)
F(6)	0.4859(7)	0.3553(8)	0.6825(4)	9.5(6)
F(7)	0.4244(7)	0.2155(8)	0.6258(5)	9.5(6)
F(8)	0.1129(7)	0.0790(8)	0.7630(5)	11.1(7)
F(9)	0.2896(8)	0.3167(8)	0.7533(6)	13.0(7)
F(10)	0.3106(7)	0.1028(8)	0.7578(6)	13.0(7)
F(11)	0.0881(8)	0.289(1)	0.7574(8)	18(1)
F(12)	0.2288(8)	0.204(1)	0.8540(4)	14.9(8)
F(13)	0.1744(9)	0.187(1)	0.6599(5)	15.6(8)
O(1)	0.9318(7)	0.0922(7)	0.5730(5)	6.3(6)
O(2)	0.7564(8)	0.0151(8)	0.5123(5)	7.8(6)
O(3)	0.7806(8)	0.0521(8)	0.6385(5)	7.5(6)
O(4)	0.5878(8)	0.1498(8)	0.4190(5)	6.7(6)
O(5)	0.633(1)	0.3406(8)	0.3858(5)	9.1(7)
O(6)	0.768(1)	0.186(1)	0.3863(5)	10.5(8)
C(1)	0.882(1)	0.345(1)	0.6088(7)	5.3(3)
C(2)	0.794(1)	0.413(1)	0.6026(7)	5.2(3)
C(3)	0.766(1)	0.448(1)	0.5301(7)	4.2(3)
C(3A)	0.849(1)	0.409(1)	0.4936(6)	4.2(3)
C(4)	0.868(1)	0.433(1)	0.4232(7)	5.7(3)
C(5)	0.958(1)	0.393(1)	0.4036(7)	6.1(4)
C(6)	1.028(1)	0.327(1)	0.4509(7)	6.0(3)
C(7)	1.012(1)	0.302(1)	0.5165(7)	5.8(3)
C(7A)	0.921(1)	0.344(1)	0.5404(6)	4.0(3)
C(8)	0.630(1)	0.254(1)	0.5809(7)	5.4(3)
C(9)	0.535(1)	0.331(1)	0.5703(8)	5.4(3)
C(10)	0.448(1)	0.317(1)	0.617(1)	7(1)
C(11)	0.988(1)	−0.011(1)	0.5913(8)	8(1)
C(12)	0.717(2)	−0.090(2)	0.521(1)	14(1)
C(13)	0.833(1)	0.079(1)	0.7088(8)	10(1)
C(14)	0.551(2)	0.076(2)	0.372(1)	19(2)
C(15)	0.557(1)	0.357(1)	0.328(1)	11(1)
C(16)	0.779(2)	0.157(2)	0.325(1)	13(1)

4. The source of the phosphonite/phosphinate complexes was confirmed by direct ^{1}H NMR observation of a quasitriplet at δ 3.95 assigned as a pair of overlapping doublets due to the diastereotopic phosphonite methoxy groups of [(η^5-indenyl)Co(C_3F_7)(PPh(*OMe*)$_2$)$_2$]$^+$ (**5e**β) on treatment of **4e** with PPh(OMe)$_2$ in acetone-d_6.

The analogous reaction of **4d** or [(η^5-indenyl)Co(C_3F_7)(PPh$_3$)(I)] with PPh(OMe)$_2$ did not afford the expected phosphinate product. Instead, a low yield (ca. 10%) of **6e**β-**1,2** along with a significant amount of uncharacterized green-blue decomposition products were obtained in both cases. We presume that preferential substitution of the bulky phosphine dominates. A diastereomeric mixture of the phosphinate **6d**β-**1,2** was successfully prepared, albeit in very low yield, via the inverse reaction of **4e** with PPh$_2$Me.

Molecular Structures of the Cobalt η^5-Cyclopentadienyl and η^5-Indenyl Phosphonate and Phosphinate Complexes. Single-crystal X-ray diffraction structures of the η^5-indenyl phosphonate **6b**α and of selected diastereomers of the η^5-cyclopentadienyl (**3b**β-**1**) and η^5-indenyl (**6b**β-**1**, **6c**β-**2**·CHCl$_3$·2.85H$_2$O) phosphinates were determined in order to confirm the structure and, in the case of the Co- and P-chiral phosphinates, to unequivocally establish the relative configuration. All structures were solved by direct methods (cf. Experimental Section for details). In each case cobalt has an unexceptional, distorted-octahedral geometry with η^5-indenyl or η^5-Cp

Table 3. Atomic Coordinates for (η^5-C_9H_7)Co(C_3F_7)(PMe_3)(P(O)(OMe)$_2$) (6bα)

atom	x	y	z	B(eq) (Å^2)
Co(1)	0.43916(7)	0.15022(3)	0.18159(4)	3.11(2)
P(1)	0.5806(2)	0.19389(8)	0.30512(8)	4.07(6)
P(2)	0.3149(2)	0.26574(7)	0.14658(8)	4.25(6)
F(1)	0.1223(3)	0.0905(2)	0.1644(1)	4.6(1)
F(2)	0.1822(3)	0.1663(2)	0.2779(2)	5.0(1)
F(3)	0.3020(4)	-0.0263(2)	0.2459(2)	6.8(2)
F(4)	0.4038(3)	0.0447(2)	0.3564(2)	6.8(2)
F(5)	0.1558(4)	-0.0553(2)	0.3719(2)	8.0(2)
F(6)	-0.0123(4)	0.0102(2)	0.2792(2)	9.5(2)
F(7)	0.1141(5)	0.0627(3)	0.3951(2)	10.3(3)
O(1)	0.4997(4)	0.2262(2)	0.3730(2)	5.3(2)
O(2)	0.7123(4)	0.1271(2)	0.3460(2)	4.7(2)
O(3)	0.6999(4)	0.2585(2)	0.2737(2)	5.6(2)
C(1)	0.5887(6)	0.1600(3)	0.0890(3)	4.0(2)
C(2)	0.6656(6)	0.1130(3)	0.1585(3)	4.4(2)
C(3)	0.5656(6)	0.0467(3)	0.1652(3)	4.0(2)
C(3A)	0.4309(5)	0.0469(3)	0.0908(3)	3.5(2)
C(4)	0.3071(6)	-0.0080(3)	0.0580(3)	4.6(2)
C(5)	0.1987(6)	0.0082(3)	-0.0175(3)	5.2(3)
C(6)	0.2113(6)	0.0784(4)	-0.0625(3)	5.4(3)
C(7)	0.3294(6)	0.1340(3)	-0.0337(3)	4.7(2)
C(7A)	0.4437(5)	0.1181(3)	0.0447(3)	3.4(2)
C(8)	0.2545(5)	0.1110(3)	0.2320(3)	3.6(2)
C(9)	0.2733(6)	0.0363(3)	0.2913(3)	4.1(2)
C(10)	0.1278(7)	0.0137(4)	0.3327(4)	5.7(3)
C(11)	0.7430(6)	0.1059(4)	0.4356(3)	6.6(3)
C(12)	0.8378(7)	0.2889(3)	0.3345(4)	7.4(3)
C(13)	0.4150(8)	0.3299(3)	0.0806(4)	6.9(3)
C(14)	0.2868(7)	0.3320(3)	0.2323(3)	5.9(3)
C(15)	0.1045(7)	0.2577(3)	0.0836(3)	6.8(3)

Table 4. Atomic Coordinates for (S_{Co},S_P/R_{Co},R_P)-(η^5-C_9H_7)Co(C_3F_7)(PMe_3)(P(O)Ph(OMe)) (6bβ-1)

atom	x	y	z	B(eq) (Å^2)
Co(1)	0.27899(7)	0.10912(7)	0.81577(6)	2.84(4)
P(1)	0.3524(1)	0.2025(2)	0.7279(1)	3.27(9)
P(2)	0.1427(1)	0.2154(2)	0.8054(1)	3.7(1)
F(1)	0.1196(3)	0.0889(3)	0.6271(3)	4.6(2)
F(2)	0.1065(3)	-0.0155(3)	0.7350(3)	4.8(2)
F(3)	0.3207(4)	-0.0065(4)	0.6291(4)	8.2(3)
F(4)	0.2725(5)	-0.1152(4)	0.7139(3)	9.3(3)
F(5)	0.2163(4)	-0.1590(4)	0.5339(3)	7.5(3)
F(6)	0.1357(5)	-0.0297(4)	0.4866(4)	9.1(3)
F(7)	0.0695(5)	-0.1215(5)	0.5686(4)	10.4(4)
O(1)	0.2801(4)	0.2346(3)	0.6316(3)	4.3(2)
O(2)	0.3929(4)	0.2913(4)	0.8018(3)	4.3(2)
C(1)	0.4035(8)	0.0137(8)	0.8836(5)	6.2(5)
C(2)	0.4322(6)	0.1034(9)	0.9187(6)	6.1(5)
C(3)	0.3592(7)	0.1361(6)	0.9640(5)	4.7(4)
C(3A)	0.2873(6)	0.0607(6)	0.9682(5)	3.6(3)
C(4)	0.2058(8)	0.0509(8)	1.0171(6)	7.0(6)
C(5)	0.157(1)	-0.034(1)	1.013(1)	10.8(9)
C(6)	0.183(1)	-0.113(1)	0.969(1)	12(1)
C(7)	0.258(1)	-0.107(1)	0.9172(7)	10.2(8)
C(7A)	0.3151(7)	-0.0187(6)	0.9190(5)	4.6(4)
C(8)	0.1849(6)	0.0351(5)	0.7034(5)	3.2(3)
C(9)	0.2352(7)	-0.0408(6)	0.6531(5)	4.3(4)
C(10)	0.1610(9)	-0.0911(7)	0.5623(7)	5.4(5)
C(11)	0.1769(6)	0.3109(6)	0.8942(6)	5.9(5)
C(12)	0.0827(7)	0.2838(6)	0.6952(6)	6.5(5)
C(13)	0.0186(6)	0.1627(7)	0.8218(7)	7.3(5)
C(14)	0.4242(7)	0.3778(6)	0.7657(7)	7.0(5)
C(15)	0.4841(5)	0.1660(5)	0.7062(5)	3.1(3)
C(16)	0.5866(6)	0.1753(6)	0.7750(5)	4.3(4)
C(17)	0.6838(6)	0.1519(6)	0.7526(6)	5.6(5)
C(18)	0.6762(7)	0.1203(7)	0.6608(7)	6.0(5)
C(19)	0.5767(7)	0.1128(7)	0.5911(6)	5.4(4)
C(20)	0.4805(6)	0.1344(6)	0.6143(5)	4.4(4)

occupying three *fac* coordination sites, as shown in Figures 4–7. Interligand bond angles P(1)–Co(1)–P(2), P(1)–Co(1)–C(8), and P(2)–Co(1)–C(8) for **6bα**, **6bβ-1**, and **6cβ-2**·$CHCl_3$·2.85H_2O; P(1)–Co(1)–P(2), P(1)–Co(1)–C(6), and P(2)–Co(1)–C(6) for **3bβ-1**) approximate 90°. Atomic

Table 5. Atomic Coordinates for (S_{Co},R_P/R_{Co},S_P)-(η^5-C_9H_7)Co(C_3F_7)($PPhMe_2$)(P(O)Ph(OMe)) (6cβ-2·$CHCl_3$·2.85H_2O)

atom	x	y	z	B(eq) (Å^2)	occ
Co(1)	0.71137(3)	0.12953(4)	0.63195(3)	3.48(3)	
P(1)	0.67932(7)	-0.0057(1)	0.61424(7)	4.10(7)	
P(2)	0.63744(7)	0.1569(1)	0.70110(6)	4.19(7)	
F(1)	0.7886(1)	0.1892(2)	0.7275(1)	4.9(2)	
F(2)	0.7478(1)	0.0653(2)	0.7555(1)	5.1(2)	
F(3)	0.8607(2)	0.0838(3)	0.6440(2)	8.8(2)	
F(4)	0.8264(2)	-0.0273(2)	0.6952(2)	8.4(2)	
F(5)	0.8635(2)	0.0627(4)	0.8052(2)	13.0(4)	
F(6)	0.9057(2)	0.1535(3)	0.7485(2)	12.1(4)	
F(7)	0.9311(2)	0.0220(3)	0.7425(2)	10.3(3)	
O(1)	0.6116(1)	-0.0093(2)	0.5990(2)	4.8(2)	
O(2)	0.6983(2)	-0.0637(2)	0.6752(2)	4.8(2)	
C(1)	0.7661(3)	0.1521(3)	0.5548(2)	4.4(3)	
C(2)	0.7042(3)	0.1407(3)	0.5339(2)	4.5(3)	
C(3)	0.6686(2)	0.2061(4)	0.5595(2)	4.4(3)	
C(3A)	0.7093(3)	0.2678(3)	0.5919(2)	4.0(3)	
C(4)	0.6990(3)	0.3512(4)	0.6203(3)	5.8(4)	
C(5)	0.7494(4)	0.3966(4)	0.6433(3)	7.1(4)	
C(6)	0.8090(4)	0.3633(5)	0.6399(3)	7.2(4)	
C(7)	0.8197(3)	0.2843(5)	0.6139(3)	5.7(4)	
C(7A)	0.7700(3)	0.2340(4)	0.5886(2)	4.1(3)	
C(8)	0.7714(2)	0.1059(3)	0.7027(2)	4.1(3)	
C(9)	0.8341(3)	0.0610(4)	0.6968(3)	5.4(4)	
C(10)	0.8833(4)	0.0722(6)	0.7500(4)	7.5(5)	
C(11)	0.7158(3)	-0.0636(3)	0.5498(3)	4.5(3)	
C(12)	0.6808(3)	-0.0825(4)	0.4955(3)	6.8(4)	
C(13)	0.7059(4)	-0.01226(6)	0.4440(3)	9.2(5)	
C(14)	0.7665(4)	-0.1454(5)	0.4457(4)	9.2(6)	
C(15)	0.8021(3)	-0.1284(5)	0.5000(4)	9.8(6)	
C(16)	0.7762(3)	-0.0871(5)	0.5515(3)	7.3(4)	
C(17)	0.6747(3)	-0.1508(4)	0.6805(3)	7.2(4)	
C(18)	0.5672(2)	0.2076(4)	0.6677(3)	4.8(3)	
C(19)	0.5280(3)	0.1590(4)	0.6290(3)	5.8(4)	
C(20)	0.4742(3)	0.1940(6)	0.6030(3)	7.7(5)	
C(21)	0.4586(4)	0.2807(7)	0.6163(4)	8.9(6)	
C(22)	0.4977(4)	0.3297(5)	0.6544(4)	8.5(5)	
C(23)	0.5516(3)	0.2948(5)	0.6804(3)	6.6(4)	
C(24)	0.6619(2)	0.2315(4)	0.7642(2)	5.7(3)	
C(25)	0.6059(2)	0.0657(4)	0.7456(2)	5.6(3)	
Cl(1)	0.4526(1)	0.0833(2)	0.0403(1)	12.0(2)	
Cl(2)	0.4804(1)	0.1189(2)	0.1709(1)	15.0(2)	
Cl(3)	0.5147(1)	0.2360(2)	0.0764(1)	16.6(2)	
C(26)	0.5047(3)	0.1269(5)	0.0957(3)	7.8(4)	
O(3)	0.068(1)	-0.003(2)	0.530(2)	15(1)	0.350
O(4)	-0.0453(7)	0.0329(8)	0.5449(7)	9.7(3)	0.550
O(5)	0.067(1)	-0.007(2)	0.494(2)	12.9(8)	0.350
O(6)	-0.000(1)	0.046(1)	0.497(1)	13.4(6)	0.350
O(7)	-0.0654(8)	0.075(1)	0.4996(9)	9.4(4)	0.350
O(8)	-0.000(1)	0.042(1)	0.5746(9)	9.7(5)	0.350
O(9)	0.0413(8)	0.378(8)	0.5721(6)	10.5(3)	0.550

coordinates, selected bond lengths, and bond angles are given in Tables 3–6 and 8–11.

Consistent with their 18e$^-$ configurations, all the π-indenyl complexes are η^5-bonded; however, small, characteristic displacements of the metal away from the C_{3a}–C_{7a} junction and distortions of the indenyl ring from planarity as observed in other formally η^5-indenyl complexes[23–27] are evident. Co displacement toward C_1–C_3 (Δ(M–C) = [average of d(M–C_{3a},C_{7a})] – [average of d(M–C_1, C_3)]) is 0.16(1) Å in **5aα**, 0.153(4) Å in **6bα**, 0.19(1) Å in **6bβ-1**, and 0.16(1) Å in **6cβ-2**·$CHCl_3$·2.85H_2O. Hinge angles of 5.8° in **5aα**, 6.7° in **6bα**, 7.3° in **6bβ-1**, and 7.0° in **6cβ-**

(23) Faller, J. W.; Crabtree, R. H.; Habib, A. *Organometallics* **1985**, *4*, 929–935.
(24) Baker, R. T.; Tulip, T. H. *Organometallics* **1986**, *5*, 839–845.
(25) Westcott, S. A.; Kakkar, A. K.; Stringer, G.; Taylor, N. J.; Marder, T. B. *J. Organomet. Chem.* **1990**, *394*, 777–794.
(26) Kakkar, A. K.; Jones, S. F.; Taylor, N. J.; Collins, S.; Marder, T. B. *J. Chem. Soc., Chem. Commun.* **1989**, 1454–1456.
(27) Kowaleski, R. M.; Rheingold, A. L.; Trogler, W. C.; Basolo, F. *J. Am. Chem. Soc.* **1986**, *108*, 2460–2461.

Table 6. Atomic Coordinates for (R_{Co},R_P/S_{Co},S_P)-(η^5-C_5H_5)Co(C_3F_7)(PMe_3)(P(O)Ph(OMe)) (3bβ-1)

atom	x	y	z	B(eq) (Å^2)
Co(1)	0.82130(6)	0.13987(3)	0.14799(3)	2.91(2)
P(1)	0.6213(1)	0.21760(5)	0.11060(7)	3.52(4)
P(2)	0.8992(1)	0.2081(6)	0.27431(6)	3.42(4)
F(1)	0.6289(3)	0.1001(1)	0.2886(1)	4.5(1)
F(2)	0.8178(3)	0.0209(1)	0.2724(1)	4.6(1)
F(3)	0.4792(3)	0.0523(1)	0.1120(2)	7.3(1)
F(4)	0.6584(3)	-0.0339(1)	0.1171(2)	6.6(1)
F(5)	0.5774(4)	-0.0735(2)	0.2884(2)	10.1(2)
F(6)	0.3982(4)	-0.0818(2)	0.1768(2)	8.3(2)
F(7)	0.3938(5)	0.0037(2)	0.2723(3)	12.1(3)
O(1)	0.7759(3)	0.2456(1)	0.3230(2)	4.5(1)
O(2)	1.0189(3)	0.2688(1)	0.2378(2)	4.8(1)
C(1)	0.8424(5)	0.0808(3)	0.0239(3)	4.5(2)
C(2)	0.9481(6)	0.0517(3)	0.0972(3)	5.0(2)
C(3)	1.0518(5)	0.1081(3)	0.1318(3)	5.2(2)
C(4)	1.0128(6)	0.1725(3)	0.0785(3)	5.2(2)
C(5)	0.8858(6)	0.1549(3)	0.0127(3)	4.9(2)
C(6)	0.7103(5)	0.0690(2)	0.2209(2)	3.5(2)
C(7)	0.5861(5)	0.0144(2)	0.1701(3)	4.1(2)
C(8)	0.4884(6)	-0.0343(3)	0.2278(3)	5.1(2)
C(9)	0.6860(6)	0.3136(3)	0.1017(4)	5.3(3)
C(10)	0.5070(7)	0.2016(3)	-0.0025(3)	5.7(3)
C(11)	0.4667(5)	0.2261(3)	0.1855(3)	4.9(2)
C(12)	1.0674(9)	0.3327(3)	0.2953(5)	8.4(4)
C(13)	1.0332(5)	0.1587(2)	0.3625(2)	3.9(2)
C(14)	0.9712(6)	0.1256(3)	0.4365(3)	5.4(2)
C(15)	1.071(1)	0.0892(3)	0.5056(4)	8.0(4)
C(16)	1.229(1)	0.0841(4)	0.5010(5)	9.6(5)
C(17)	1.2924(7)	0.1156(4)	0.4281(5)	8.4(4)
C(18)	1.1957(6)	0.1535(3)	0.3597(3)	5.8(3)

Table 7. Selected Bond Distances (Å) and Bond Angles (deg) for [(η^5-C_9H_7)Co(C_3F_7)($P(OMe)_3$)$_2$]$^+$$SbF_6^-$ (5aα-SbF_6)

Co(1)–P(1)	2.205(4)	C(3A)–C(7A)	1.41(1)
Co(1)–P(2)	2.187(4)	C(4)–C(5)	1.36(2)
Co(1)–C(1)	2.09(1)	C(5)–C(6)	1.41(2)
Co(1)–C(2)	2.07(1)	C(6)–C(7)	1.33(1)
Co(1)–C(3)	2.09(1)	C(7)–C(7A)	1.41(1)
Co(1)–C(3A)	2.24(1)	C(8)–C(9)	1.52(2)
Co(1)–C(7A)	2.25(1)	C(9)–C(10)	1.54(2)
Co(1)–C(8)	1.95(1)	P(1)–O(1)	1.581(9)
C(1)–C(2)	1.39(2)	P(1)–O(2)	1.578(9)
C(1)–C(7A)	1.45(1)	P(1)–O(3)	1.566(9)
C(2)–C(3)	1.42(2)	P(2)–O(4)	1.555(9)
C(3)–C(3A)	1.44(1)	P(2)–O(5)	1.56(1)
C(3A)–C(4)	1.42(1)	P(2)–O(6)	1.60(1)
P(1)–Co(1)–P(2)	96.0(2)	P(2)–Co(1)–C(3)	100.4(4)
P(1)–Co(1)–C(1)	92.5(4)	P(2)–Co(1)–C(3A)	89.6(3)
P(1)–Co(1)–C(2)	124.4(4)	P(2)–Co(1)–C(7A)	111.9(3)
P(1)–Co(1)–C(3)	158.0(4)	P(2)–Co(1)–C(8)	95.2(4)
P(1)–Co(1)–C(3A)	127.9(3)	C(1)–Co(1)–C(8)	113.0(5)
P(1)–Co(1)–C(7A)	95.5(3)	C(2)–Co(1)–C(8)	89.1(5)
P(1)–Co(1)–C(8)	89.8(4)	C(3)–Co(1)–C(8)	103.0(5)
P(2)–Co(1)–C(1)	150.6(4)	C(3A)–Co(1)–C(8)	141.3(5)
P(2)–Co(1)–C(2)	139.5(4)	C(7A)–Co(1)–C(8)	151.5(5)

2·$CHCl_3$·2.85H_2O between the planes defined by C_1–C_2–C_3 and C_1–C_3–C_{3a}–C_{7a} as well as fold angles of 11.0° in **5aα**, 10.0° in **6bα**, 11.4° in **6bβ-1**, and 10.5° in **6cβ-2**·$CHCl_3$·2.85H_2O between the plane C_1–C_2–C_3 and the best plane containing C_{3a}–C_4–C_5–C_6–C_7–C_{7a} (Table 15) are consistent with a moderate distortion compared to the values for a range of reported indenyl complexes.[11,12,23,25-27]

NMR Spectroscopy of the η^5-Cyclopentadienyl and η^5-Indenyl Phosphonate and Phosphinate Complexes. Complete ^{1}H, ^{31}P, ^{13}C, and ^{19}F NMR parameters for the η^5-indenyl and η^5-cyclopentadienyl phosphonate and phosphinate complexes isolated in this study are given in Tables 12–14. ^{31}P NMR is an excellent diagnostic for characterization of a phosphoryl group.[6] All phosphonate and phosphinate complexes **3** and **6** showed well-resolved ^{31}P AB patterns (cf. Table 12). Coordinated $P(OMe)_3$ (δ 145 ± 2 ppm for neutral complexes **6aα**, **6′aα**, **3aα**) and $PPh(OMe)_2$ (δ 170 ± 2 ppm for **6eβ**) were considerably less shielded than P(O)$(OMe)_2$ (δ 73–93 ppm for **3aα**, **3bα**, **6aα**, **6′aα**, **6bα**, and **6cα**) and P(O)Ph(OMe) (δ 97–112 ppm for **6bβ**, **6cβ**, **6dβ**, and **6eβ**).

The most interesting features in the ^{1}H and ^{13}C NMR spectra of the phosphinate and phosphonate complexes are derived from the presence of chiral P and/or Co centers which require that pairs of indenyl ring atoms (1,3; 4,7; 5,6; cf. Chart 1 for numbering) as well as geminal substituents CX_2 (X = OMe, F) be diastereotopic. Large

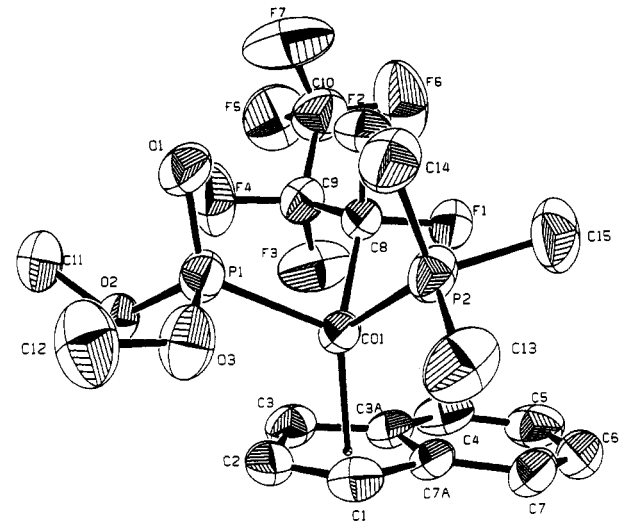

Figure 4. ORTEP representation of (η^5-indenyl)Co(C_3F_7)-(PMe_3)(P(O)$(OMe)_2$) (**6bα**).

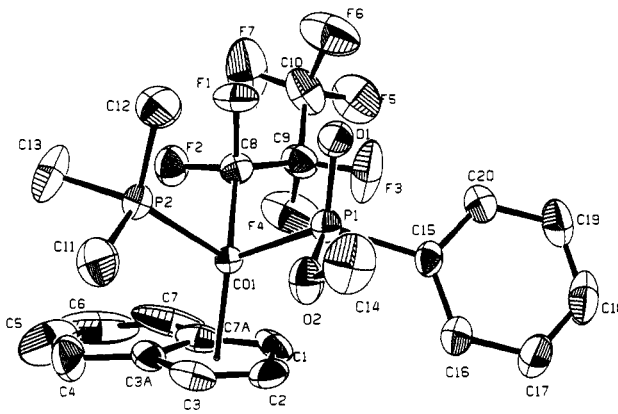

Figure 5. ORTEP representation of (S_{Co},S_P/R_{Co},R_P)-(η^5-indenyl)Co(C_3F_7)(PMe_3)(P(O)Ph(OMe)) (**6bβ-1**) (S_{Co},S_P enantiomer shown).

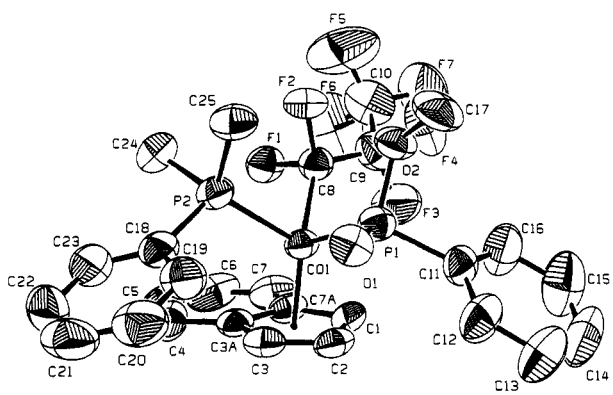

Figure 6. ORTEP representation of (S_{Co},R_P/R_{Co},S_P)-(η^5-indenyl)Co(C_3F_7)($PPhMe_2$)(P(O)Ph(OMe)) (**6cβ-2**·$CHCl_3$·2.85H_2O) (S_{Co},R_P enantiomer shown).

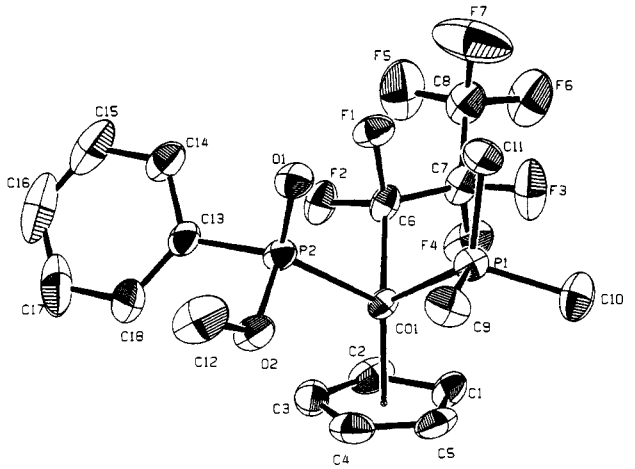

Figure 7. ORTEP representation of ($R_{Co}R_P/S_{Co}S_P$)-(η^5-Cp)-$Co(C_3F_7)(PMe_3)$(P(O)Ph(OMe)) (**3b**β-**1**) ($R_{Co}R_P$ enantiomer shown).

Table 8. Selected Bond Distances (Å) and Bond Angles (deg) for (η^5-C_9H_7)$Co(C_3F_7)(PMe_3)(P(O)(OMe)_2)$ (6bα)

Co(1)–P(1)	2.186(1)	C(3A)–C(7A)	1.426(6)
Co(1)–P(2)	2.229(1)	C(4)–C(5)	1.362(7)
Co(1)–C(1)	2.104(4)	C(5)–C(6)	1.402(7)
Co(1)–C(2)	2.071(4)	C(6)–C(7)	1.366(7)
Co(1)–C(3)	2.086(4)	C(7)–C(7A)	1.419(6)
Co(1)–C(3A)	2.258(4)	C(8)–C(9)	1.565(6)
Co(1)–C(7A)	2.238(4)	C(9)–C(10)	1.527(7)
Co(1)–C(8)	1.972(4)	P(1)–O(1)	1.479(3)
C(1)–C(2)	1.399(6)	P(1)–O(2)	1.609(3)
C(1)–C(7A)	1.442(6)	P(1)–O(3)	1.617(4)
C(2)–C(3)	1.412(6)	P(2)–C(13)	1.818(6)
C(3)–C(3A)	1.441(6)	P(2)–C(14)	1.812(5)
C(3A)–C(4)	1.399(6)	P(2)–C(15)	1.817(5)
P(1)–Co(1)–P(2)	93.20(5)	P(2)–Co(1)–C(3)	157.9(1)
P(1)–Co(1)–C(1)	108.2(1)	P(2)–Co(1)–C(3A)	125.0(1)
P(1)–Co(1)–C(2)	85.8(1)	P(2)–Co(1)–C(7A)	94.2(1)
P(1)–Co(1)–C(3)	102.0(1)	P(2)–Co(1)–C(8)	92.6(1)
P(1)–Co(1)–C(3A)	140.5(1)	C(1)–Co(1)–C(8)	156.6(2)
P(1)–Co(1)–C(7A)	146.4(1)	C(2)–Co(1)–C(8)	139.9(2)
P(1)–Co(1)–C(8)	93.9(1)	C(3)–Co(1)–C(8)	102.2(2)
P(2)–Co(1)–C(1)	93.6(1)	C(3A)–Co(1)–C(8)	93.9(2)
P(2)–Co(1)–C(2)	127.5(2)	C(7A)–Co(1)–C(8)	118.4(2)

Chart 1. Numbering Scheme for Indenyl

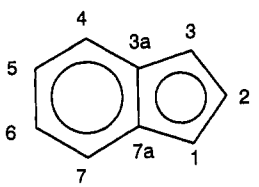

diastereotopic chemical shift differences of the indenyl ring and geminal phosphonate methoxyl resonances gave well-separated resonances in both the 7.05-T ^1H and ^{13}C NMR spectra. Intra-ring proton couplings were in general not resolved. Unequivocal ^1H and ^{13}C NMR assignments (cf. Tables 12 and 13) were possible on the basis of the ^1H nuclear Overhauser effect difference (NOED) spectra, which measured sequential NOE enhancements around the ring perimeter, and 2-D $^1H/^{13}C$ ^1J heterocorrelation spectra. The ^{13}C chemical shift assignments permitted calculation of $\Delta\delta(^{13}C_{3a,7a})$ distortion parameters (Table 15)-which fall in the range −22 to −15 ppm for all π-indenyl complexes characterized in this study. Both solution NMR and solid-state crystallographic evidence (*vide infra*) support a moderately distorted η^5-indenyl coordination mode.[12,13,24-26,28]

Table 9. Selected Bond Distances (Å) and Bond Angles (deg) for ($S_{Co}S_P/R_{Co}R_P$)-(η^5-C_9H_7)$Co(C_3F_7)$-(PMe_3)(P(O)Ph(OMe)) (6bβ-1)

Co(1)–P(1)	2.207(2)	C(3A)–C(4)	1.417(9)
Co(1)–P(2)	2.247(2)	C(3A)–C(7A)	1.42(1)
Co(1)–C(1)	2.072(8)	C(4)–C(5)	1.34(2)
Co(1)–C(2)	2.055(8)	C(5)–C(6)	1.37(2)
Co(1)–C(3)	2.102(7)	C(6)–C(7)	1.37(1)
Co(1)–C(3A)	2.267(7)	C(7)–C(7A)	1.43(1)
Co(1)–C(7A)	2.283(8)	P(1)–O(1)	1.482(5)
Co(1)–C(8)	1.987(7)	P(1)–O(2)	1.617(5)
C(1)–C(2)	1.36(1)	P(1)–C(15)	1.854(6)
C(1)–C(7A)	1.43(1)	P(2)–C(11)	1.810(8)
C(2)–C(3)	1.36(1)	P(2)–C(12)	1.812(8)
C(3)–C(3A)	1.41(1)	P(2)–C(13)	1.812(8)
P(1)–Co(1)–P(2)	90.73(8)	P(2)–Co(1)–C(8)	91.9(2)
P(1)–Co(1)–C(1)	105.2(3)	C(1)–Co(1)–C(8)	103.3(4)
P(1)–Co(1)–C(2)	88.2(2)	C(2)–Co(1)–C(8)	140.3(4)
P(1)–Co(1)–C(3)	108.5(3)	C(3)–Co(1)–C(8)	155.1(3)
P(1)–Co(1)–C(3A)	145.6(2)	C(3A)–Co(1)–C(8)	118.2(3)
P(1)–Co(1)–C(7A)	143.2(2)	C(7A)–Co(1)–C(8)	94.2(3)
P(1)–Co(1)–C(8)	95.5(2)	Co(1)–P(1)–O(1)	118.0(2)
P(2)–Co(1)–C(1)	156.6(2)	Co(1)–P(1)–O(2)	100.7(2)
P(2)–Co(1)–C(2)	127.6(4)	Co(1)–P(1)–C(15)	119.0(2)
P(2)–Co(1)–C(3)	94.3(2)	O(1)–P(1)–O(2)	111.4(3)
P(2)–Co(1)–C(3A)	94.3(2)	O(1)–P(1)–C(15)	104.9(3)
P(2)–Co(1)–C(7A)	124.3(2)	O(2)–P(1)–C(15)	101.6(3)

Table 10. Selected Bond Distances (Å) and Bond Angles (deg) for ($S_{Co}R_P/R_{Co}S_P$)-(η^5-C_9H_7)$Co(C_3F_7)$-$(PPhMe_2)$(P(O)Ph(OMe)) (6cβ-2·$CHCl_3$·2.85H_2O)

Co(1)–P(1)	2.200(2)	C(3A)–C(4)	1.426(7)
Co(1)–P(2)	2.257(2)	C(3A)–C(7A)	1.423(7)
Co(1)–C(1)	2.086(5)	C(4)–C(5)	1.370(8)
Co(1)–C(2)	2.078(5)	C(5)–C(6)	1.399(9)
Co(1)–C(3)	2.109(5)	C(6)–C(7)	1.345(8)
Co(1)–C(3A)	2.266(5)	C(7)–C(7A)	1.413(7)
Co(1)–C(7A)	2.256(5)	P(1)–O(1)	1.500(3)
Co(1)–C(8)	1.979(5)	P(1)–O(2)	1.600(3)
C(1)–C(2)	1.414(7)	P(1)–C(11)	1.831(5)
C(1)–C(7A)	1.437(7)	P(2)–C(18)	1.830(6)
C(2)–C(3)	1.386(7)	P(2)–C(24)	1.815(5)
C(3)–C(3A)	1.443(7)	P(2)–C(25)	1.825(5)
P(1)–Co(1)–P(2)	93.01(6)	P(2)–Co(1)–C(8)	90.7(2)
P(1)–Co(1)–C(1)	102.1(2)	C(1)–Co(1)–C(8)	103.7(2)
P(1)–Co(1)–C(2)	84.0(1)	C(2)–Co(1)–C(8)	140.0(2)
P(1)–Co(1)–C(3)	105.4(2)	C(3)–Co(1)–C(8)	155.1(2)
P(1)–Co(1)–C(3A)	143.4(1)	C(3A)–Co(1)–C(8)	116.9(2)
P(1)–Co(1)–C(7A)	140.5(1)	C(7A)–Co(1)–C(8)	93.8(2)
P(1)–Co(1)–C(8)	98.9(2)	Co(1)–P(1)–O(1)	111.9(2)
P(2)–Co(1)–C(1)	157.1(1)	Co(1)–P(1)–O(2)	108.0(1)
P(2)–Co(1)–C(2)	127.1(2)	Co(1)–P(1)–C(11)	115.6(2)
P(2)–Co(1)–C(3A)	93.5(1)	O(1)–P(1)–O(2)	111.9(2)
P(2)–Co(1)–C(3A)	93.8(1)	O(1)–P(1)–C(11)	106.0(2)
P(2)–Co(1)–C(7A)	124.3(1)	O(2)–P(1)–C(11)	103.1(2)

The perfluoropropyl C_α–C_γ ^{19}F NMR resonances (cf. Table 14) are well resolved in both the η^5-indenyl and η^5-cyclopentadienyl series. Typically small vicinal couplings ($^3J_{FF}$ = 5–10 Hz) allow an approximation of the ^{19}F spectra of the diastereotopic $C_\alpha F_2$ and $C_\beta F_2$ groups as isolated AB spin systems with $^2J_{F_aF_b}$ = 265–290 Hz.[7,12,13] The coupling constants $^2J_{F_aF_b}$ show a marked increase on passing from C_α to C_β but are relatively constant farther along the perfluoroalkyl chain,[12,13] suggesting a weakening of the C_α–F bond.[29] All complexes have a larger diastereotopic chemical shift difference ($\Delta\delta(F_aF_b) = \delta(F_a) - \delta(F_b)$ (ppm)) for $C_\alpha F_aF_b$ than for $C_\beta F_aF_b$. Except for the diastereomeric pair **6b**β-**1,2**, $\Delta\delta(F_aF_b)$ for C_α and C_β is larger

(28) Marder, T. B.; Calabrese, J. C.; Roe, D. C.; Tulip, T. H. *Organometallics* **1987**, *6*, 2012–2014.
(29) Karel, K. J.; Tulip, T. H.; Ittel, S. D. *Organometallics* **1990**, *9*, 1276–1282.

Table 11. Selected Bond Distances (Å) and Bond Angles (deg) for (R_{Co},R_P/S_{Co},S_P)-(η^5-C_5H_5)Co(C_3F_7)-(PMe_3)(P(O)Ph(OMe)) (3bβ-1)

Co(1)–P(1)	2.208(1)	C(2)–C(3)	1.391(6)
Co(1)–P(2)	2.233(1)	C(3)–C(4)	1.404(7)
Co(1)–C(1)	2.116(4)	C(4)–C(5)	1.382(6)
Co(1)–C(2)	2.097(4)	P(1)–C(9)	1.815(5)
Co(1)–C(3)	2.078(4)	P(1)–C(10)	1.820(5)
Co(1)–C(4)	2.101(4)	P(1)–C(11)	1.813(5)
Co(1)–C(5)	2.122(4)	P(2)–O(1)	1.494(3)
Co(1)–C(6)	1.968(4)	P(2)–O(2)	1.622(3)
C(1)–C(2)	1.401(6)	P(2)–C(13)	1.829(4)
C(1)–C(5)	1.394(6)		
P(1)–Co(1)–P(2)	89.67(4)	P(2)–Co(1)–C(6)	91.3(7)
P(1)–Co(1)–C(1)	104.6(1)	C(1)–Co(1)–C(6)	103.5(2)
P(1)–Co(1)–C(2)	143.2(1)	C(2)–Co(1)–C(6)	90.3(2)
P(1)–Co(1)–C(3)	148.1(2)	C(3)–Co(1)–C(6)	114.0(9)
P(1)–Co(1)–C(4)	108.9(2)	C(4)–Co(1)–C(6)	152.8(2)
P(1)–Co(1)–C(5)	88.4(1)	C(5)–Co(1)–C(6)	141.0(2)
P(1)–Co(1)–C(6)	97.7(1)	Co(1)–P(2)–O(1)	118.9(1)
P(2)–Co(1)–C(1)	157.6(1)	Co(1)–P(2)–O(2)	103.3(1)
P(2)–Co(1)–C(2)	126.2(2)	Co(1)–P(2)–C(13)	113.7(1)
P(2)–Co(1)–C(3)	93.4(1)	O(1)–P(2)–O(2)	111.0(2)
P(2)–Co(1)–C(4)	94.4(1)	O(1)–P(2)–C(13)	107.2(2)
P(2)–Co(1)–C(5)	127.3(1)	O(2)–P(2)–C(13)	101.2(2)

in the higher R_f complexes compared to the lower R_f complexes.

Stereochemistry of the Cobalt(III) η^5-Indenyl and η^5-Cyclopentadienyl Phosphinate Complexes. Assignments of relative configuration at Co and P for the diastereomeric pairs **6bβ-1**, **6cβ-2**, and **3bβ-1**, necessary to establish the nature of the Co→P chiral induction, are based on crystallographic data. The ORTEP molecular structure representation in Figure 5 and the modified Cahn–Ingold–Prelog[30–33] ligand priority series η^5-indenyl/η^5-Cp > P(O)Ph(OMe) > PMe_3 > C_3F_7 and Co > OMe > O > Ph establish that cobalt and phosphorus have the same relative configuration (S_{Co},S_P/R_{Co},R_P) in the higher R_f diastereomer **6bβ-1** and therefore that the lower R_f diastereomer **6bβ-2** has the opposite relative configuration at cobalt and phosphorus (S_{Co},R_P/R_{Co},S_P). Similarly, the relative configuration of lower R_f diastereomer **6cβ-2** (Figure 6) is S_{Co},R_P/R_{Co},S_P and that of the higher R_f diasteromer, **6cβ-1**, is S_{Co},S_P/R_{Co},R_P. The relative configurations for the higher R_f diasteromer **3bβ-1** (Figure 7) and lower R_f diasteromer **3bβ-2** are R_{Co},R_P/S_{Co},S_P and R_{Co},S_P/S_{Co},R_P, respectively, and were assigned using the same procedure.

Relative configurations at Co and P for the diastereomeric pairs **6dβ-1,2** and **6eβ-1,2** were empirically determined by comparison of chromatographic R_f and NMR chemical shift parameters for the chiral phosphorus center. As summarized in Table 16, each pair of diastereomers shows the same NMR chemical shift pattern: δ(^{1}H, ^{13}C, and $^{31}P_{P(O)OMe}$, (high R_f)) > δ(^{1}H, ^{13}C, and $^{31}P_{P(O)OMe}$ (low R_f)). Accordingly, the relative configurations for the higher R_f diastereomers **6dβ-1** and **6eβ-1** can be assigned as S_{Co},S_P/R_{Co},R_P and those for the lower R_f diastereomers **6dβ-2** and **6eβ-2** are S_{Co},R_P/R_{Co},S_P. Interestingly, the direction of chiral induction in the reaction of **4c** and PPh(OMe)$_2$, which gives **6cβ-1,2** (cf. Scheme 3), is opposite that found for the other cases examined in this study. The major product is low-R_f (S_{Co},R_P/R_{Co},S_P)-**6cβ-2**, with the same relative configuration as the minor products for the remaining examples in Schemes 2 and 3.

Conformational Analysis. The solution conformations of the phosphonate and phosphinate complexes were probed using ^{1}H NOED experiments. If the transition state for Arbuzov dealkylation (**2** → **3** and **5** → **6**) at prochiral phosphorus is productlike to a significant degree, restricted rotations about the Co–P(O) and Co–indenyl bonds in **3** and **6** emerge as critical determinants for Co→P chiral transmission. Complexes **3bα**, **6bα**, **3bβ-1**, and **6bβ-1** are illustrative.

Solution ^{1}H NOED evidence establishes a preferred conformation about the Co–indenyl bond for the π-indenyl complexes **6**. Partial saturation of P*Me*$_3$ in **6bα** results in strong enhancements to H_1 (4.2%) and H_7 (2.8%) but no enhancement to H_2 and H_3. Irradiation of the diastereotopic P–O*Me* groups shows specific enhancement (1.1%) to H_2. For **6bβ-1**, partial saturation of the indenyl H_1, H_2, and H_3 protons shows 2.2%, 4.3%, and 0.3% enhancements to the H_{ortho} protons of P(O)*Ph*(OMe), respectively. The same relative enhancement order (5.1%, 6.9%, and 1.2% enhancements to H_1, H_2, and H_3) was obtained on irradiation of H_{ortho} of P(O)*Ph*(OMe). Together with the strong correlations to H_1 (3.5%) and H_7 (6.4%) when P*Me*$_3$ is irradiated, the NOED results establish restricted rotation about the Co–indenyl bond and population of a major rotamer with P(O)(OMe)$_2$ or P(O)Ph(OMe) *trans* to the indenyl six-ring.

Figure 8 summarizes the NOED correlations measured for the indenyl phosphonate and phosphinate complexes **6**. Both solid-state and solution evidence concur that the dominant rotamer places phosphinate or phosphonate *anti* to the indenyl six-ring. Although steric effects are critical in substituted cyclopentadienyl three-legged piano stools,[34–36] our results conclude that ligand steric requirements are not the primary determinant of conformational preference about the Co–indenyl ring centroid bond. Arguments have been made[23,37] which suggest that the ligand with highest *trans* influence prefers the site *anti* to the indenyl six-ring in order to maximize aromatization. The *trans*-influence order for the ligand set examined here can be estimated as P(O)R(OMe) > C_3F_7 ≥ phosphine,[38,39] suggesting that this interpretation has merit. Of the nine literature examples where the solid-state or solution conformation of (η^5-indenyl)M(X)(Y)(Z) (X, Y, and Z are 2e$^-$ σ donors) complexes was determined,[23,34,40–43] seven showed the same conformation established for the phosphonate and phosphinate complexes **6** with the highest *trans* influence ligand *anti* to the indenyl six-ring. Although steric effects mitigate in some instances, the sole exception appears with the ligand set X, Y, Z = PPh_2N-

(30) Cahn, R. S.; Ingold, C.; Prelog, V. *Angew. Chem., Int. Ed. Engl.* **1966**, *5*, 385–415.
(31) Stanley, K.; Baird, M. C. *J. Am. Chem. Soc.* **1975**, *97*, 6598–6599.
(32) Sloan, T. E. *Top. Stereochem.* **1981**, *12*, 1–36.
(33) Mata, P.; Lobo, A. M.; Marshall, C.; Johnson, A. P. *Tetrahedron: Asymmetry* **1993**, *4*, 657–668.
(34) Loonat, M. S.; Carlton, L.; Boeyens, J. C. A.; Coville, N. J. *J. Chem. Soc., Dalton Trans.* **1989**, 2407–2414.
(35) Coville, N. J.; Loonat, M. S.; White, D.; Carlton, L. *Organometallics* **1992**, *11*, 1082–1090.
(36) Du Plooy, K. E.; Marais, C. F.; Carlton, L.; Hunter, R.; Boeyens, J. C. A.; Coville, N. J. *Inorg. Chem.* **1989**, *28*, 3855–3860.
(37) Crabtree, R. H.; Parnell, C. P. *Organometallics* **1984**, *3*, 1727–1731.
(38) Bao, Q. B.; Brill, T. B. *Inorg. Chem.* **1987**, *26*, 3447–3452.
(39) Appleton, T. G.; Clark, H. C.; Manzer, L. E. *Coord. Chem. Rev.* **1973**, *10*, 335–422.
(40) Foo, T.; Bergman, R. G. *Organometallics* **1992**, *11*, 1801–1810.
(41) Pannell, K.; Castillo-Ramirez, J.; Cervantes-Lee, F. *Organometallics* **1992**, *11*, 3139–3143.
(42) Oro, L. A.; Ciriano, M. A.; Campo, M.; Foces-Foces, C.; Cano, F. H. *J. Organomet. Chem.* **1985**, *289*, 117–131.
(43) Brunner, H.; Fisch, K.; Jones, P. G.; Salbeck, J. *Angew. Chem., Int. Ed. Engl.* **1989**, *28*, 1521–1522.

Table 12. ^{1}H and ^{31}P NMR for Cobalt(III) η^5-Cyclopentadienyl and η^5-Indenyl Complexes[a,b]

compd	H_1	H_2	H_3	H_4	H_5	H_6	H_7	Cp	Me	C_6H_5	^{31}P
1b[c]								5.32	1.83 (d, 11.4)		16.38
1b'								5.46	1.70 (t, 5.4)		14.83
3aα								5.23	3.76 (d, 10.9)[d], 3.66 (d, 10.7)[e], 3.67 (d, 10.9)[e]		146.12 (d, 104.2)[q], 73.00 (d, 169.4)[r]
3bα								5.10	1.58 (d, 11.1)[f], 3.66 (d, 10.9)[e], 3.67 (d, 9.6)[e]		22.71 (d, 117.1)[s], 92.29 (m)[r]
5aα	6.10	5.71	6.10	*g*	*g*	*g*	*g*		3.75 (t, 5.4)		135.34
6aα	5.36	5.87 (m)[h]	5.79	7.39 (m)	7.30 (m)	7.30 (m)	7.46 (m)		3.62 (d, 10.4)[d], 3.63 (d, 10.7)[e], 3.65 (d, 10.3)[e]		144.70 (d, 119.3)[q], 85.44 (d, 163.2)[r]
6'aα	5.35	5.88 (m)[h]	5.79	7.39 (m)	7.31 (m)	7.31 (m)	7.45 (m)		3.62 (d, 10.4)[d], 3.64 (d, 10.7)[e], 3.66 (d, 10.2)[e]		144.45 (d, 140.9)[q], 84.94 (d, 164.6)[r]
6bα	5.07	5.97 (m)[h]	5.87	7.46 (m)	7.37 (m)	7.30 (m)	7.38 (m)		1.33 (d, 11.0)[f], 3.63 (d, 10.6),[e] 3.65 (d, 10.8)[e]		13.47,[s] 84.04[r]
6cα	4.17	5.86	5.75	7.36 (m)	7.29 (m)	7.29 (m)	6.95 (m)		1.27 (d, 10.6),[f] 1.61 (d, 11.3),[f] 3.71 (d, 10.6),[e] 3.77 (d, 10.7)[e]	7.98 (m, 2 H),[i] 7.55 (m, 3H)[j,k]	17.17 (d, 94.2),[s] 83.35 (d, 83.9)[r]
3bβ-1								5.04	1.65 (d, 11.1),[f] 3.50 (d, 10.9)[e]	7.68 (m, 2H),[i] 7.37 (m, 3H)[m,n]	22.5 (d, 105.8),[s] 111.58 (d, 103.5)[r]
3bβ-2								4.89	1.66 (d, 11.1),[f] 3.39 (d, 11.1)[e]	7.80 (m, 2H),[i] 7.42 (m, 3H),[m,n]	22.01 (d, 104.9),[s] 105.63 (d, 102.3)[r]
6bβ-1	5.39	5.72	5.67	7.35[o]	7.28	7.28	7.35[o]		1.28 (d, 11.1),[f] 3.52 (d, 10.7)[e]	7.72 (m, 2H),[i] 7.35 (m, 3H)[m,n]	13.82 (d, 85.0),[s] 104.09 (d, 88.8)[r]
6bβ-2	5.03	5.20 (m)	5.61 (m)	7.37 (m)	7.48 (m)[o]	7.37 (m)	7.37 (m)		1.42 (d, 11.0),[f] 3.29 (d, 11.4)[e]	7.86 (m, 2H),[i] 7.48 (m, 2H),[m] 7.29 (m, 1H)[n]	13.85 (d, 85.0),[s] 100.74 (d, 114.6)[r]
6cβ-1	4.70	6.08	5.49	7.30 (m)	7.13 (t, 7.5)	6.97 (t, 7.5)	6.64 (d, 8.3)		1.38 (d, 11.1),[f] 1.88 (d, 11.1),[f] 3.50 (d, 10.8)[e]	7.70 (m, 4H),[i,j] 7.47 (m, 3H), 7.40 (m, 3H)	17.79 (d, 45.7),[s] 103.17 (d, 77.8)[r]
6cβ-2	4.17	5.11	5.23	7.29 (m)	7.29 (m)	7.29 (m)	7.07 (m)		1.42 (d, 10.5),[f] 1.81 (d, 11.4),[f] 3.34 (d, 11.4)[e]	8.26 (m, 2H),[i] 7.96 (m, 2H),[i] 7.55 (m, 3H),[i,k] 7.49 (m, 3H)[m,n]	15.89 (d, 40.2),[s] 103.04 (d, 70.5)[r]
6dβ-1	5.08	6.17 (m)	5.63	7.45 (m)	7.14 (t, 7.7)	6.64 (t, 7.7)	6.45 (d, 8.3)		1.93 (dd, 11.5, 2.6),[f] 2.94 (d, 10.9)[e]	7.92 (m, 2H),[i] 6.79 (m, 2 H),[i] 7.53 (m, 2H),[i] 7.50 (m, 3H), 7.30 (m, 4H), 7.18 (m, 2H)	34.17 (d, 87.5),[s] 98.70 (d, 101.3)[r]
6dβ-2	4.79	5.45 (m)	5.39 (m)	7.56 (m)[o]	7.24 (t, 7.9)	7.13 (t, 7.6)	6.53 (d, 8.3)		1.86 (d, 10.2),[f] 2.91 (d, 11.3)[e]	7.78 (m, 2 H),[i] 7.72 (m, 4H),[i] 7.30–7.56 (m, 9H)	20.52 (d, 78.4),[s] 97.71 (d, 72.2)[r]
6eβ-1	4.87	6.13	5.90	7.35 (m)	7.18 (m)	7.18 (m)	7.05 (m)		3.27 (dd, 10.6, 1.8),[e] 3.42 (d, 9.1),[d] 3.46 (d, 8.9)[d]	8.15 (m, 2H),[i] 7.36 (m, 2H),[i] 7.52 (m, 3H),[j,k] 7.28 (m, 3H)[m,n]	106.71 (d, 108.6),[r] 168.99 (d, 77.5)[q]
6eβ-1	5.04	5.49	5.49	7.29 (m)	*p*	*p*	*p*		3.21 (d, 11.2),[e] 3.52 (d, 11.0),[d] 3.62 (d, 10.7)[d]	7.76–7.90 (m, 4H),[i,l] 7.38–7.50 (m, 6H)	100.69 (d, 105.3),[r] 172.23 (d, 75.1)[q]

[a] Conditions and definitions: ^{1}H (300.1 MHz) NMR chemical shifts in ppm relative to TMS; ^{31}P (121.5 MHz) NMR chemical shifts in ppm relative to external 85% H_3PO_4; J_{PP} in Hz given in parentheses; all peaks show further unresolved splitting; solvent $CDCl_3$; m = multiplet; d = doublet; t = triplet. [b] All indenyl proton peaks show further small, unresolved coupling (0.3–1.5 Hz). [c] Solvent acetone-d_6. [d] $PR(OMe)_2$, $^3J_{PH}$. [e] P(O)R(OMe), $^3J_{PH}$. [f] P–Me, $^2J_{PH}$. [g] Appear as a multiplet center at 7.54 ppm. [h] J = 3–5 Hz. [i] H_{ortho} of P–Ph. [j] H_{meta} of P–Ph. [k] H_{para} of P–Ph. [l] H_{ortho} of P(O)–Ph. [m] H_{meta} of P(O)–Ph. [n] H_{para} of P(O)–Ph. [o] Overlapped with phenyl protons. [p] 7.10–7.23 (m, 3H). [q] $PR(OMe)_2$. [r] $P(O)R(OMe)$. [s] PPh_nMe_{3-n}.

(Me)CH(Me)Ph, Me, CO,[43] where the strongest *trans* influence ligand, Me, lies under the indenyl six-ring.

Strong intramolecular hydrogen bonding (Scheme 1) in the aminophosphine-substituted phosphonate and phosphinate analogs studied previously constrained the Co—P(O) conformation by forcing L = $PPh_2NHCH(Me)Ph$ and P=O to be *syn*.[2-5,7] Since intramolecular hydrogen bonding is not possible for the phosphonates and phosphinates prepared in this study, it was of interest to examine the conformation about the Co—P(O) bond. In the solid state, phosphonate **6bα** and both $S_{Co},S_P/R_{Co},R_P$ phosphinate complexes **6bβ-1** and **3bβ-1** adopt a staggered conformation similar to that for the aminophosphine derivatives of Scheme 1, in which the phosphoryl P=O double bond is aligned *anti* to the indenyl or cyclopentadienyl plane, as shown in the Newman projections of Figure 9A–C. For **6bβ-1** and **3bβ-1** the P(O)*Ph*(OMe) phenyl group is *syn* and "edge-on" to the indenyl or cyclopentadienyl plane. The solid-state conformation of ($S_{Co},R_P/R_{Co},S_P$)-**6cβ-2**, the major diastereomer for L = $PPhMe_2$, does not follow the pattern (cf. Figure 9D); however, a similar edge-on phenyl/indenyl interaction occurs by placing the OMe group *anti* to the indenyl moiety. NOED evidence suggests that the solid-state conformation about the Co—P(O) bond persists in solution. Partial saturation of either diastereotopic OMe resonance in **6bα** results in enhancement of the indenyl H_2 signal consistent with a conformation in which both

Table 13. ^{13}C NMR for Cobalt(III) η^5-Cyclopentadienyl and η^5-Indenyl Complexes[a]

compd	C_1	C_2	C_3	C_{3a}/C_{7a}	C_4	C_5	C_6	C_7	C_8	C_6H_5	Me
1b[b]									88.07		19.94 (d, 34.8)
1b'									90.88		22.15 (t, 16.0)
3aα									89.44		53.96 (d, 8.0),[c] 51.27 (d, 8.8),[d] 50.92 (d, 8.7)[d]
3bα									88.85		19.60 (d, 32.6),[e] 51.49 (d, 9.1),[d] 50.51 (d, 10.6)[d]
5aα	76.40	97.92	76.40	111.43	126.80	132.59	132.59	126.80			55.60 (d, 4.5)
6aα	75.46	99.01	73.75 (t, 5.0)	113.99, 110.81 (d, 4.4)	126.24	129.25	128.51	126.07			53.77 (d, 7.5),[c] 51.75 (d, 10.7),[d] 51.58 (d, 10.5)[d]
6'aα	75.50	99.14	73.95 (t, 5.0)	114.11, 110.77	126.35	129.29	128.56	126.10			53.84 (d, 8.7),[c] 51.83 (d, 8.7),[d] 51.64 (d, 8.7)[d]
6bα	74.60	100.43	72.53 (t, 6.3)	113.74, 110.64 (d, 4.8)	127.33 (d, 4.5)	129.35	128.76	123.20			16.59 (d, 30.6),[e] 51.75 (d, 7.2),[d] 51.65 (d, 7.2)[d]
6cα	79.62	99.18	71.40	114.37 (d, 3.3), 109.19 (d, 8.7)	126.89 (d, 5.0)	129.36	129.07	122.28		139.36 (d, 44.6),[f] 130.62,[g] 130.51,[g] 129.98,[h] 128.42,[i] 128.31[i]	10.94 (d, 26.7),[e] 17.81 (d, 28.3),[e] 51.89 (d, 11.1)[d]
3bβ-1									88.65	132.28 (d, 55.2),[f] 130.83,[g] 130.69,[g] 129.30,[h] 127.60,[i] 127.45[i]	19.34 (d, 33.1),[e] 50.41 (d, 8.7)[d]
3bβ-2									89.63	134.48 (d, 51.1),[f] 130.55,[g] 130.40,[g] 129.40,[h] 127.89,[i] 127.74[i]	19.63 (d, 32.4),[e] 49.57 (d, 12.5)[d]
6bβ-1	75.08	98.35	73.85	112.92, 112.86	126.04	129.43	128.90	125.46		142.11 (d, 53.9),[f] 130.96,[g] 130.82,[g] 128.85,[h] 127.69,[i] 127.56[i]	16.07 (d, 32.3),[e] 50.79 (d, 10.8)[d]
6bβ-2	75.34	100.96	71.83 (d, 4.0)	114.70, 111.70	126.60	129.67	128.93[j]	123.35		141.80 (d, 55.6),[f] 130.48,[g] 130.35,[g] 129.93,[h] 128.02,[i] 127.89[i]	16.50 (d, 29.0),[e] 50.23 (d, 11.8)[d]
6cβ-1	75.31	97.40	73.74	115.42, 113.11	127.19 (d, 8.9)	129.97	128.49	121.89		138.58 (d, 41.2),[f] 131.03,[g] 130.90,[g] 130.72,[g] 130.62,[g] 129.67,[h] 129.54,[h] 128.23,[i] 128.11,[i] 127.73,[i] 127.60[i]	13.51 (d, 27.7),[e] 16.81 (d, 32.4),[e] 51.11 (d, 10.5)[d]
6cβ-2	82.44	99.92	69.77 (t, 6.1)	116.57, 109.06 (t, 6.1)	125.92	129.85[h]	128.58	122.59		139.71 (d, 45.5),[f] 132.59 (d, 43.7),[f] 131.14,[g] 131.04,[g] 130.86,[g] 130.73,[g] 130.04,[h] 129.85,[h] 128.62,[i] 128.44[i]	11.98 (d, 26.2),[e] 17.18 (d, 30.6),[e] 50.46 (d, 13.2)[d]
6dβ-1	75.45	96.99	74.02		127.52			121.30		127.62–133.94	17.50 (d, 25.5),[e] 51.01 (d, 8.5)[d]
6dβ-2	77.50	98.34	70.74					120.45		126.80–134.75	16.86 (d, 24.2),[e] 49.98 (d, 10.3)[d]
6eβ-1	76.10	102.77	74.54 (t, 8.2)	113.00, 112.91	127.20 (d, 8.5)	129.43	129.30	123.46		140.50 (d, 53.5),[f] 137.50 (d, 53.2),[f] 132.28,[g] 132.17,[g] 132.00,[g] 131.83,[g] 131.21,[h] 128.74,[h] 127.90,[i] 127.77,[i] 126.66,[i] 126.51[i]	51.57 (d, 11.6),[d] 53.94 (d, 14.3),[c] 54.09 (d, 8.8)[c]
6eβ-2	78.27	99.93	73.62	115.70, 111.61	125.89	129.52	128.71	124.63		142.40 (d, 54.3),[f] 135.73 (d, 53.5),[f] 132.09,[g] 131.94,[g] 130.89,[g] 130.76,[g] 130.89,[h] 129.52,[h] 127.59,[i] 127.71[i]	50.70 (d, 11.4),[d] 54.77 (d, 12.1),[c] 54.9 (d, 14.9)[c]

[a] Conditions and definitions: ^{13}C (75.47 MHz) NMR chemical shifts in ppm relative to solvent $CDCl_3$ (77.0 ppm); d = doublet; J values in Hz given in parentheses, J_{PC}; perfluoroalkyl carbons distributed in the chemical shift range 105–140 ppm with very weak intensity. [b] Solvent acetone-d_6 (29.8, 206.0 ppm). [c] $PR(OMe)_2$. [d] P(O)R(OMe). [e] P–Me. [f] C_{ipso}. [g] C_{ortho}. [h] C_{para}. [i] C_{meta}. [j] Overlapped with C_{para}.

methoxy groups are *syn* with respect to the indenyl ring. As described above for the case of **6bβ-1**, significant NOE enhancements were measured between the indenyl protons H_1, H_2, and H_3 and H_{ortho} of P(O)*Ph*(OMe); hence, Ph is *syn* to the indenyl residue.

Threefold torsional barriers for rotation about M–ligand bonds in three-legged piano-stool complexes have been discussed by several authors.[44-49] The simple steric model favored by Davies[46] minimizes eclipsing interactions and,

(44) Mackie, S. C.; Park, Y. S.; Shurvell, H. F.; Baird, M. C. *Organometallics* **1991**, *10*, 2993–2995.
(45) Mackie, S. C.; Baird, M. C. *Organometallics* **1992**, *11*, 3712–3724.
(46) Blackburn, B. K.; Davies, S. G.; Whittaker, M. In *Stereochemistry of Organometallic and Inorganic Compounds*; Bernal, I., Ed.; Elsevier: Amsterdam, 1989; Vol. 3, Chapter 2, pp 141–223.
(47) Crowe, W. E.; Schreiber, S. L. In *Advances in Metal-Organic Chemistry*; Liebeskind, L., Ed.; JAI Press: London, 1991; Vol. 2, pp 247–267.
(48) Shambayati, S.; Crowe, W. E.; Schreiber, S. L. *Angew. Chem., Int. Ed. Engl.* **1990**, *29*, 256–272.
(49) Garner, E.; Orpen, A. G. *J. Chem. Soc., Dalton Trans.* **1993**, 533–541.

Table 14. ^{19}F NMR for Cobalt(III) η^5-Cyclopentadienyl and η^5-Indenyl Complexes[a]

compd	$C_\alpha F_2$ F_a, F_b	$C_\beta F_2$ F_a, F_b	CF_3
1b[b]	−60.90, −70.89 (d, 267.2)	−112.78, −113.29 (d, 282.1)	−78.20 (t, 11.9)
1b′	−66.28	−113.98	−78.98 (t, 11.5)
3aα	−61.51, −71.82 (d, 258.8)	−111.77, −115.92 (d, 281.35)	−79.33 (t, 12.7)
3bα	−65.91, −72.25 (d, 268.2)	−113.37, −115.05 (d, 280.9)	−78.99 (t, 12.8)
5aα	−60.62 (m)	−113.82	−79.43 (t, 10.7)
6aα	−71.49, −72.93 (d, 263.4)	−114.92	−79.19 (t, 10.5)
6′aα[c]	−70.42, −72.24 (d, 272.1)	−110.29, −111.07 (d, 291.0)	−81.36 (t, 8.7)
6bα	−73.28, −81.40 (d, 261.6)	−113.65, −115.96 (d, 282.2)	−79.17 (t, 11.0)
6cα	−73.78, −82.51 (d, 266.1)	−114.24, −115.92 (d, 282.7)	−79.22 (t, 12.8)
3bβ-1	−62.66, −77.70 (d, 269.3)	−112.34, −115.08 (d, 276.6)	−79.08 (t, 10.0)
3bβ-2	−63.08, −74.17 (d, 267.4)	−112.40, −114.50 (d, 279.2)	−79.00 (t, 9.8)
6bβ-1	−72.61	−114.02	−79.17 (t, 10.5)
6bβ-2	−73.72, −78.67 (d, 273.9)	−113.98	−79.26 (t, 10.7)
6cβ-1	−71.18, −79.96 (d, 278.7)	−112.80, −114.64 (d, 277.4)	−79.16
6cβ-2	−76.16, −79.58 (d, 273.2)[d]	−113.24, −114.71 (d, 275.8)	−79.49
6dβ-1	−66.27, −81.04 (d, 290.0)	−112.76, −115.71 (d, 277.6)	−78.78
6dβ-2	−71.10, −74.76 (d, 275.0)	−113.51, −113.69	−79.29
6eβ-1	−67.06, −73.63 (d, 271.8)	−111.85, −115.23 (d, 280.5)[e]	−79.04 (t, 10.9)
6eβ-2	−70.77, −71.60 (d, 272.0)	−113.31, −113.91 (d, 277.1)	−79.43 (t, 11.0)

[a] Conditions and definitions: 282.4 MHz, chemical shifts in ppm relative to $CFCl_3$; solvent $CDCl_3$; $^2J_{PF_aF_b}$, and $^3J_{FF}$ in the case of CF_3, in Hz given in parentheses; all CF_2 peaks show further unresolved splitting by about 5–10 Hz (three and more bond coupling). [b] Solvent acetone-d_6. [c] $C_\gamma F_2$: F_a, F_b = −121.10, −121.85 (d, 314.2). $C_\delta F_2$: −123.04. $C_\epsilon F_2$: F_a, F_b = −126.55. [d] $C_\alpha F_a$ shows further doublet with J = 39.0 Hz. [e] $C_\beta F_a$ shows further doublet with J = 9.8 Hz.

Table 15. Distortion Parameters in Cobalt(III) η^5-Indenyl Complexes

compd	$\Delta\delta(C_{3a,7a})$[a] (av)	Δ(M–C)[b] (Å)	hinge angle[c] (deg)	fold angle[d] (deg)
5aα	−19.27	0.16(1)	5.8	11.0
6aα	−16.71, −19.89 (−18.30)			
6′aα	−16.59, −19.93 (−18.26)			
6bα	−16.96, −20.06 (−18.51)	0.153(4)	6.7	10.0
6cα	−16.33, −21.51 (−18.92)			
6bβ-1	−17.78, −17.84 (−17.81)	0.19(1)	7.3	11.4
6bβ-2	−16.00, −19.00 (−17.50)			
6cβ-1	−15.28, −17.59 (−16.44)			
6cβ-2	−14.13, −21.64 (−17.89)	0.16(1)	7.0	10.5
6eβ-1	−17.70, −17.79 (−17.75)			
6eβ-2	−15.00, −19.09 (−17.05)			

[a] $\Delta\delta(C_{3a,7a}) = \delta[C_{3a,7a}(\text{indenyl})] - \delta[C_{3a,7a}(Na^+\text{indenyl}^-)]$, $\delta[C_{3a,7a}(Na^+\text{indenyl}^-)] = 130.70$ ppm.[24,25] [b] Δ(M–C) = [average of d(M–$C_{3a,7a}$)] – [average of d(M–$C_{1,3}$)]. [c] Hinge angle = dihedral angle between the least-squares planes C(1)–C(2)–C(3) and C(1)–C(3)–C(3a)–C(7a). [d] Fold angle = dihedral angle between the least-squares planes C(1)–C(2)–C(3) and C(3a)–C(4)–C(5)–C(6)–C(7)–C(7a).

Table 16. Determination of the Relative Configurations for Cobalt η^5-Indenyl and η^5-Cyclopentadienyl Phosphonate Complexes[a]

	$S_{Co}S_P/R_{Co}R_P$, high R_f (TLC)	$S_{Co}R_P/R_{Co}S_P$, low R_f (TLC)
	(η^5-C_9H_7)Co(C_3F_7)(PMe_3)(P(O)Ph(OMe))	
isomer	**6bβ-1**	**6bβ-2**
^{1}H NMR	3.52	3.29
^{13}C NMR	50.79	50.23
^{31}P NMR	104.09	100.74
X-ray	yes	
	(η^5-C_9H_7)Co(C_3F_7)($PPhMe_2$)(P(O)Ph(OMe))	
isomer	**6cβ-1**	**6cβ-2**
^{1}H NMR	3.50	3.34
^{13}C NMR	51.11	50.46
^{31}P NMR	103.17	103.04
X-ray		yes
	(η^5-C_9H_7)Co(C_3F_7)(PPh_2Me)(P(O)Ph(OMe))	
isomer	**6dβ-1**	**6dβ-2**
^{1}H NMR	2.94	2.91
^{13}C NMR	51.01	49.98
^{31}P NMR	98.70	97.71
X-ray		
	(η^5-C_9H_7)Co(C_3F_7)($PPh(OMe)_2$)(P(O)Ph(OMe))	
isomer	**6eβ-1**	**6eβ-2**
^{1}H NMR	3.27	3.21
^{13}C NMR	51.57	50.70
^{31}P NMR	106.71	100.69
X-ray		
	(η^5-C_5H_5)Co(C_3F_7)(PMe_3)(P(O)Ph(OMe))	
isomer	**3bβ-1**	**3bβ-2**
^{1}H NMR	3.50	3.39
^{13}C NMR	50.41	49.57
^{31}P NMR	111.58	105.63
X-ray	yes	

[a] ^{1}H and ^{13}C NMR data are the chemical shifts in ppm for P(O)Ph(O*Me*); ^{31}P NMR data are the chemical shifts for *P*(O)Ph(OMe).

as a consequence of the near 90° interligand bond angles, identifies the site *anti* to π-Cp′ as least sterically accessible. In agreement with our results for **6bα**, **6bβ-1**, and **3bβ-1**, predictions based on a crude extension of the Davies model which neglects stereoelectronic as well as dipole effects and assumes the steric sequence L > Cp or indenyl > R_f predicts that the lowest energy rotamer will place the least sterically demanding phosphoryl oxygen *anti* to Cp or indenyl and, in the case of the phosphinates, the P(O)-*Ph*(OMe) phenyl substituent *anti* to the largest Co-bound substituent, L (cf. Figure 9). The major conformer adapted by **6cβ-2** is clearly not predicted from simple steric arguments, since methoxy rather than oxygen occupies the least sterically accessible site. In this case, however, to force oxygen into the preferred site by a rotation of 120° would incur an unfavorable *syn* interaction between the phenyl substituents of P(O)Ph(OMe) and L = $PPhMe_2$. The conformation found for **6cβ-2** reasonably represents the best compromise between constraints imposed by steric parameters and noncovalent (phenyl/Cp edge-on) interactions.[50]

Optical Yields for Scheme 3. Nucleophilic attack of displaced iodide on the diastereotopic OMe groups of **2** and **5** proceeds with low to moderate Co*→P chiral induction. Small but characteristic differences in the ^{1}H NMR η^5-Cp, η^{-5}-indenyl, and methoxy chemical shifts (^{1}H NMR: δ 3.2–3.5 ppm, $^3J_{PH}$ = 10 ± 1 Hz) apparent for the diastereomeric phosphinate products were indispensable

(50) Bernal, I.; Reisner, G. M.; Brunner, H.; Riepl, G. *J. Organomet. Chem.* **1985**, *284*, 115–128.

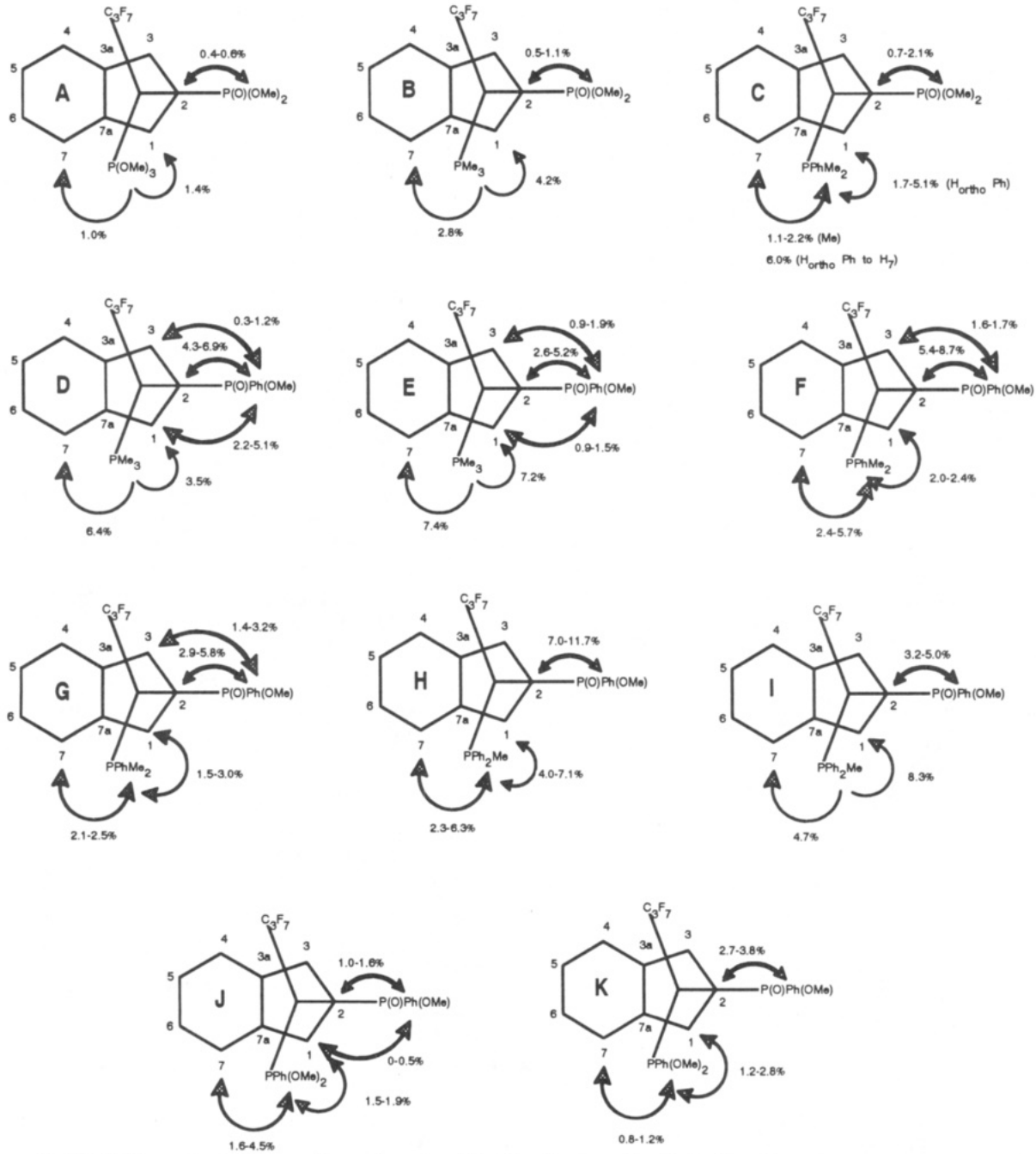

Figure 8. NOE data and solution conformation: **6aα** (A); **6bα** (B); **6cα** (C); **6bβ-1** (D); **6bβ-2** (E); **6cβ-1** (F); **6cβ-2** (G); **6dβ-1** (H); **6dβ-2** (I); **6eβ-1** (J); **6eβ-2** (K).

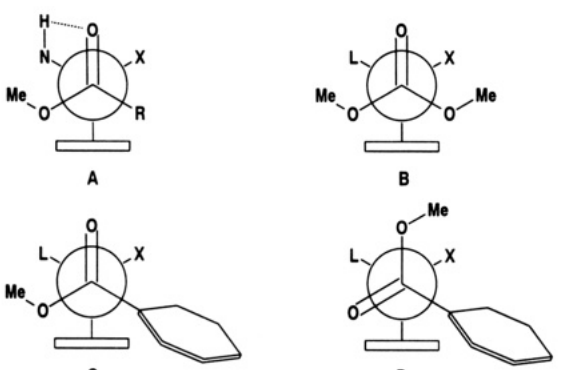

Figure 9. Newman projections of the phosphonate and phosphinate complexes along the P(O)–Co bond.

for measuring kinetic product distributions. ^{1}H NMR determination of product ratios gave a diastereotopic excess of 4%, 27%, 48%, 46%, and 35% de for **6bβ-1**/**6bβ-2**, **3bβ-1**/**3bβ-2**, **6cβ-2**/**6cβ-1**, **6dβ-1**/**6dβ-2**, and **6eβ-1**/**6eβ-2**, respectively. Optical yields are lower than that observed in the reaction between aminophosphine-substituted iodo analogs (η^5-Cp)Co(PNH)(I)$_2$ and PPh(OMe)$_2$ (80% de)[2] but, with the exception of **5bβ**, are compatible with the percent de in the reaction between (η^5-Cp)Co(R$_f$)(PNH)(I) and PPh(OMe)$_2$ (R$_f$ = CF$_3$, C$_3$F$_7$; 25–55% de).[4]

Several interesting features are evident from consideration of the optical yield data. We had anticipated that removal of conformational restraints imposed by intramolecular hydrogen bonding (cf. Scheme 1) would result in reduced efficacy of chiral information transfer from cobalt to phosphorus. Although a nominal decrease was observed using the reaction of (η^5-Cp)Co(PNH)(I)$_2$ with PPh(OMe)$_2$ as a reference,[2] no measurable decrease results with a

Table 17. Summary of Crystallographic Data

	5aα-SbF_6	6bα	6bβ-1	6cβ-2·$CHCl_3$·2.85H_2O	3bβ-1
formula	$C_{18}H_{25}O_6CoF_{13}P_2Sb$	$C_{17}H_{22}O_3CoF_7P_2$	$C_{22}H_{24}O_2CoF_7P_2$	$[C_{27}H_{26}O_2CoF_7P_2{\cdot}CHCl_3]{\cdot}2.85H_2O$	$C_{18}H_{22}O_2CoF_7P_2$
mol wt	827.00	528.23	574.30	807.09	524.24
color; habit	orange rect plate	deep red prism	red rect plate	red prism	orange prism
cryst size (mm)	0.30 × 0.20 × 0.15	0.30 × 0.25 × 0.12	0.35 × 0.25 × 0.20	0.40 × 0.30 × 0.10	0.40 × 0.30 × 0.15
cryst syst	monoclinic	monoclinic	monoclinic	monoclinic	monoclinic
space group	$P2_1/c$ (No. 14)	$P2_1/c$ (No. 14)	$P2_1/c$ (No. 14)	$C2/c$ (No. 15)	$P2_1/c$ (No. 14)
a (Å)	12.821(4)	8.235(2)	12.626(20	21.794(8)	8.481(4)
b (Å)	12.057(3)	16.983(3)	14.017(7)	15.214(2)	17.916(3)
c (Å)	18.835(4)	15.795(2)	14.380(2)	21.115(3)	14.518(2)
β (deg)	99.74(2)	101.88(1)	107.46(1)	92.33(2)	97.31(2)
V (Å^3)	2869(10	2161.6(7)	2428(1)	6995(3)	2188(1)
Z	4	4	4	8	4
D_{calc} (g/cm^3)	1.914	1.623	1.571	1.533	1.591
F_{000}	1624	1072	1168	3284	1064
μ(Mo Kα) (cm^{-1})	17.48	10.10	9.04	8.80	9.95
scan width (deg)	1.31 + 0.30 tan θ	1.15 + 0.30 tan θ	1.26 + 0.30 tan θ	1.00 + 0.30 tan θ	1.26 + 0.30 tan θ
$2\theta_{max}$ (deg)	50.0	50.0	50.0	50.0	50.0
no. of rflns measd					
total	4524	4242	4675	6580	4269
unique	4272	3952	4462	6398	3986
R_{int}	0.209	0.024	0.063	0.021	0.034
cor[a]			Lorentz, polarization, abs		
transmissn factors	0.94–1.00	0.93–1.00	0.89–1.00	0.86–1.00	0.92–1.00
secondary extn coeff		0.16748 × 10^{-6}			0.19909 × 10^{-6}
p factor	0.01	0.01	0.01	0.00	0.01
no. of obsd ($I > 3.00\sigma(I)$)	1913 ($I > 2.00\sigma(I)$)	2455	2158	3961 ($I > 2.00\sigma(I)$)	2780
no. of variables	315	272	307	416	338
rfln/param	6.07	9.03	7.03	9.52	8.22
R[b]	0.055	0.038	0.051	0.052	0.036
R_w[c]	0.039	0.034	0.040	0.036	0.033
GOF[d]	1.81	1.76	1.85	2.60	1.83
max shift error in final cycle	0.00	0.00	0.02	0.00	0.03
$\Delta\rho$ final (max/min) (ϵ/Å^3)	+0.51/–0.46	+0.36/–0.22	+0.74/–0.44	+0.59/–0.48	+0.41/–0.39

[a] See ref 53. [b] $R = \sum||F_o| - |F_c||/\sum|F_o|$. [c] $R_w = [(\sum w(|F_o| - |F_c|)^2/\sum wF_o^2)]^{1/2}$. [d] GOF = $(\sum(|F_o| - |F_c|)\sigma)/(n - m))$ where n is the number of reflections, m is the number of variables, and σ^2 is the variance of $(|F_o| - |F_c|)$. Function minimized: $\sum w(|F_o| - |F_c|)^2$. Least-squares weights: $4F_o^2/\sigma^2(F_o^2)$.

reference reaction of (η^5-Cp)Co(R_f)(PNH)(I) and PPh(OMe)$_2$ (R_f = CF_3, C_3F_7).[4] Also surprising is the observation of a *reversal* in relative stereochemistry of the major diastereomer formed in the reaction of **4c** with PPh(OMe)$_2$. We are currently investigating the potential of MMX molecular mechanics[45,51] calculations to address the more subtle steric interactions implicit in these data but cannot provide a convincing rationale for the direction of the reported optical inductions at this time.

Experimental Section

Reagents and Methods. All reactions were performed under a dry, oxygen-free nitrogen atmosphere using standard Schlenk techniques. Nitrogen gas was purified by passing through a series of columns containing DEOX (Alfa) catalyst heated to 120 °C, granular P_4O_{10}, and finally activated 3A molecular sieves. Benzene, hexane, and pentane solvents were distilled under nitrogen from blue solutions of sodium benzophenone ketyl. Methylene chloride was distilled under nitrogen from P_4O_{10}, acetone and ethyl acetate from 4A molecular sieves (4–8 mesh), and methanol from NaOH. Spectrograde chloroform was used as received. P(OMe)$_3$ was purchased from Strem and distilled before use. PPh(OMe)$_2$ and PMe_3 were purchased from Strem and used as received. Thin-layer chromatographic analyses were performed on precoated TLC plates (silica gel F-254, Merck). Thick-layer radial chromatographic separations were carried out using a Chromatotron (Harrison Associates) with 1, 2, or 4 mm thick silica gel$_{60}$$PF_{254}$ (Merck) adsorbent. Elemental analyses were performed by Canadian Microanalytical Service Ltd. (Delta, BC, Canada). Melting points were determined in nitrogen-sealed capillaries and are uncorrected. NMR spectra were recorded on a GE 300-NB Fourier transform spectrometer operating at a proton frequency of 300.12 MHz. Proton NOED spectra were determined under steady-state conditions on the GE 300-NB instrument as previously described.[2] Complexes **1a**[7] and **4a–e** and **4′a**[12] were prepared as described previously.

X-ray Crystallography. Crystal data for **5aα**-SbF_6, **6bα**, **6bβ-1**, **6cβ-2**·$CHCl_3$·2.85H_2O, and **3bβ-1** were collected at ambient temperature on a Rigaku AFC6S diffractometer with graphite-monochromated Mo Kα radiation (λ = 0.710 69 Å) and a 2-kW sealed-tube generator using the ω–2θ scan technique to a maximum 2θ value of 50.0°. Space group assignments were based on systematic absences and on the successful solution and refinement of the structure. Weak reflections ($I < 10.0\sigma(I)$) were rescanned (max 2) and the counts accumulated to assure good counting statistics. For **5aα**-SbF_6, **6bα**, **6bβ-1**, and **3bβ-1** the intensities of 3 representative reflections measured after every 150 reflections remained constant throughout the data collection; hence, no decay corrections were applied. In the case of **6cβ-2**·$CHCl_3$·2.85H_2O intensities of 3 representative reflections measured after every 150 reflections declined by 3.10%; hence, a linear correction factor was applied. The data were corrected for Lorentz and polarization effects. Structures were solved by direct methods,[52] using the Molecular Structure Corp. TEXSAN software. Non-hydrogen atoms were refined anisotropically. Idealized hydrogen atoms were included at the calculated positions but were not refined. Further details are given in Table 17.

Synthesis of [(η^5-C_9H_7)Co(C_3F_7)(P(OMe)$_3$)$_2$]$^+$$SbF_6^-$ (5aα). A solution prepared by dissolving 0.3952 g (1.150 mmol) of $AgSbF_6$ in 40 mL of acetone was slowly added via syringe into a stirred solution of **4a**, (η^5-C_9H_7)Co(C_3F_7)(I)(P(OMe)$_3$) (0.6610 g, 1.113 mmol), in 25 mL of the same solvent over a 30-min period at room temperature. After the mixture was stirred for an additional 30 min, the yellow AgI precipitate was filtered off through a

(51) Polowin, J.; Mackie, S. C.; Baird, M. C. *Organometallics* **1992**, *11*, 3724–3730.

(52) Gilmore, C. J. *J. Appl. Crystallogr.* **1984**, *17*, 42–46.

(53) Walker, N.; Stuart, D. *Acta Crystallogr., Sect. A: Found Crystallogr.* **1983**, *A39*, 158–166.

Schlenk filter fitted with a 5-cm Celite pad. $P(OMe)_3$ (0.1987 g, 1.601 mmol) was added to the filtrate via syringe and the solution stirred for 30 min. Removal of volatiles by aspirator followed by oil pump vacuum left an orange powder, which was dissolved in 5 mL of acetone and purified by thick-layer radial chromatography with acetone/hexane (7/5, v/v) as eluent. Removal of solvent from the first yellow band left **5aα** as an orange-yellow crystalline solid (0.8720 g, 95%). A crystalline specimen for X-ray characterization was prepared by slow diffusion of pentane into the CH_2Cl_2 solution of **5aα** at 0 °C.

Synthesis of (η^5-C_5H_5)Co(C_3F_7)(I)(PMe_3) (1b). PMe_3 (0.1714 g, 2.253 mmol) was added dropwise via syringe with stirring to a dark green solution of (η^5-C_5H_5)Co(C_3F_7)(I)(CO) (0.9541 g, 2.130 mmol) in 25 mL of benzene at room temperature. After the mixture was stirred for 5 min, a dark blue solution containing some precipitate formed. Removal of solvent at aspirator pressure left a dark blue powder. TLC analysis (benzene/hexane 2/1) showed dark blue (R_f 0.33) and yellow (R_f 0) products. The crude product was purified in several portions by thick-layer radial chromatography with benzene/hexane (5/1 v/v) as eluent, the initial dark blue band being collected. Continued elution with acetone separated a yellow band. Removal of solvent from the combined dark blue eluates gave **1b** (0.7299 g, 69%) as a dark blue powder. Removal of solvent from the combined yellow eluates gave a yellow powder (0.0862 g), which was crystallized by slow diffusion of hexane into the acetone solution and identified as [(η^5-C_5H_5)Co(C_3F_7)(PMe_3)$_2$]$^+$I$^-$ (**1b′**).

Synthesis of (η^5-Cp-η^5-C_9H_7)Co(R_f)(L)(P(O)(OMe)$_2$) (3aα, 3bα, 6aα, 6′aα, 6bα, and 6cα). The phosphonate complexes were synthesized by adding a slight excess of $P(OMe)_3$ to the appropriate iodide (η^5-Cp-η^5-C_9H_7)Co(R_f)(L)(I) in benzene or acetone solution at room temperature and then heating. The reaction progress was followed by observing a color change to yellow (η^5-Cp) or red (η^5-indenyl) using a procedure similar to that described for **6aα** below.

$P(OMe)_3$ (0.0830 g, 0.669 mmol) was added via syringe with stirring to a solution of **4a** (0.2566 g, 0.4319 mmol) in 25 mL of benzene at ambient temperature. Heating the solution to reflux resulted in a color change from brown-red to red after ca. 0.5 h. Removal of solvent by aspirator and then oil pump vacuum left the product as a red, pastelike solid. Crude **6aα** was dissolved in ca. 3 mL of acetone and purified by thick-layer radial chromatography with acetone/methanol (20/1 v/v) as eluent. Removal of the solvent from the last orange-yellow band by aspirator and then oil pump vacuum afforded **6aα** as a red powder (0.1941 g, 78%). Experimental parameters for the remaining phosphonate complexes are summarized in Table 18.

Synthesis of (η^5-C_9H_7)Co(C_3F_7)($PPhMe_2$)(P(O)Ph(OMe)) (6cβ-1,2). $PPh(OMe)_2$ (0.0741 g, 0.436 mmol) was added slowly via syringe to a stirred solution of **4c**, (η^5-C_9H_7)Co(C_3F_7)(I)($PPhMe_2$) (0.2170 g, 0.3568 mmol), in 20 mL of benzene at ambient temperature. Heating to 50 °C for about 5 h resulted in a color change from brown-red to red. TLC (ethyl acetate elution) of the crude reaction mixture showed four spots corresponding (in order of decreasing R_f value) to a low-yield, uncharacterized product, **6cβ-1,2**, and the mixture of a disubstituted species (**6eβ**). Removal of solvent by aspirator and then oil pump vacuum left a red pastelike solid, which was dissolved in 3 mL of ethyl acetate and chromatographed on a 2-mm radial silica gel plate. Ethyl acetate elution separated **6cβ-1** and **6cβ-2** as orange bands. Continued elution with ethyl acetate/methanol (20/1) separated yellow zones of the disubstituted byproducts. Removal of the solvent with water aspirator and then oil pump vacuum afforded **6cβ-1** (0.0328 g, 14%), **6cβ-2** (0.1058 g, 47%), **6eβ-1** (0.0098 g), and **6eβ-2** (0.0135 g) as red powders. Slow diffusion of hexane into a $CHCl_3$ solution of **6cβ-2**·$CHCl_3$·2.85H_2O at room temperature gave red prismatic crystals for X-ray analysis.

Table 18. Preparative Parameters for the Reactions of 1 and 4 with $PR(OMe)_2$ (R = OMe, Ph)[a]

compd	solvent	reacn temp (°C)/ time (h)	mole ratio ($PR(OMe)_2$/ reactant)	chromatography solvent	yield (%)
3aα	benzene	reflux/15	1.42	acetone/ methanol (10/1)	87
3bα	acetone	50/10	1.29		96
6aα	benzene	reflux/0.5	1.55	acetone/ methanol (20/1)	78
6′aα	benzene	reflux/0.5	1.55	acetone/ methanol (20/1)	85
6bα	benzene	50/4	1.09	acetone/ methanol (20/1)	90[b]
6cα	benzene	50/0.5	2.25	acetone	89[b]
3bβ-1,2	aetone	50/3	2.10	acetone/ methanol (10/1)	64, 31[c]
6bβ-1,2	benzene	50/5	1.17	acetone	58, 28
6cβ-1,2	benzene	50/5	1.22	ethyl acetate	14, 47[d]
6eβ-1,2	benzene	22/14	1.35	ethyl acetate/ methanol (20/1)	35, 27

[a] Crystal growth conditions: slow diffusion of hexane into the solution of **6bα** (methylene chloride, room temperature), **6bβ-1** (methylene chloride, 0 °C), **6cβ-2** (chloroform, room temperature), and **3bβ-1** (acetone, 0 °C). [b] Minor amounts of **6aα** were also isolated in the lower R_f fractions. [c] **3eβ-1,2**[4] were detected in the crude product mixture. [d] Continued elution with ethyl acetate/methanol (20/1) separated **6eβ-1** (4%) and **6eβ-2** (6%).

Synthesis of (η^5-C_9H_7)Co(C_3F_7)(PPh_2Me)(P(O)Ph(OMe)) (6dβ-1,2) PPh_2Me (0.0594 g, 0.297 mmol) was added via syringe with stirring to a brown-red solution of **4e**, (η^5-C_9H_7)Co(C_3F_7)(I)($PPh(OMe)_2$) (0.1463 g, 0.2285 mmol), in 25 mL of benzene and stirred for 14 h at room temperature. TLC (ethyl acetate/methylene chloride 1/1) showed that **4e** was converted mainly into **4d**, **6eβ-1,2**, and uncharacterized R_f 0 material. Only very small amounts of **6dβ-1** and **6dβ-2** were detected. After removal of volatiles at aspirator pressure the residue was chromatographed on a 2-mm radial silica gel plate. Elution with ethyl acetate/methylene chloride (1/1) separated **6dβ-1,2** from **4d**, **6eβ-1,2**, and the decomposed material. Rechromatographing the **6dβ-1,2** mixture with ethyl acetate/methylene chloride (1/1) as eluent gave **6dβ-1** (8.3 mg, 5%) and **6dβ-2** (3.0 mg, 2%) as a red powder. Experimental parameters for the remaining phosphinate complexes are summarized in Table 18.

Acknowledgment. We thank the Natural Sciences and Engineering Research Council of Canada (NSERC) for financial support of this work. Z.Z. acknowledges Memorial University for a graduate fellowship.

Supplementary Material Available: Tables of experimental details of the X-ray studies, least-squares planes and deviations therefrom, positional parameters for the H atoms, B(eq) and U values, all bond distances and angles, torsion or conformation angles, and intermolecular distances and figures offering additional views of **5aα**, **6bα**, **6bβ-1**, **6cβ-2**, and **3bβ** (155 pages). Ordering information is given on any current masthead page.

OM9305733